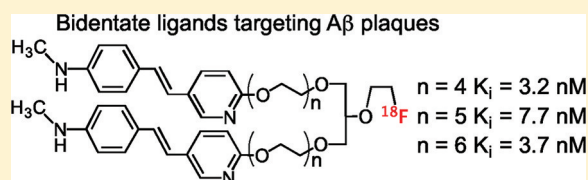


Multidentate  $^{18}\text{F}$ -Polypegylated Styrylpyridines As Imaging Agents for  $\text{A}\beta$  Plaques in Cerebral Amyloid Angiopathy (CAA)Zhihao Zha,<sup>†</sup> Seok Rye Choi,<sup>§</sup> Karl Ploessl,<sup>†</sup> Brian P. Lieberman,<sup>†</sup> Wenchao Qu,<sup>†</sup> Franz Hefti,<sup>§</sup> Mark Mintun,<sup>§</sup> Daniel Skovronsky,<sup>†,§</sup> and Hank F. Kung<sup>\*,†,‡</sup><sup>†</sup>Departments of Radiology and <sup>‡</sup>Pharmacology, University of Pennsylvania, Philadelphia, Pennsylvania 19104, United States<sup>§</sup>Avid Radiopharmaceuticals Inc., Philadelphia, Pennsylvania 19104, United States

## Supporting Information

**ABSTRACT:**  $\beta$ -Amyloid plaques ( $\text{A}\beta$  plaques) in the brain are associated with cerebral amyloid angiopathy (CAA). Imaging agents that could target the  $\text{A}\beta$  plaques in the living human brain would be potentially valuable as biomarkers in patients with CAA. A new series of  $^{18}\text{F}$  styrylpyridine derivatives with high molecular weights for selectively targeting  $\text{A}\beta$  plaques in the blood vessels of the brain but excluded from the brain parenchyma is reported. The styrylpyridine derivatives, **8a–c**, display high binding affinities and specificity to  $\text{A}\beta$  plaques ( $K_i = 2.87, 3.24,$  and  $7.71$  nM, respectively). In vitro autoradiography of [ $^{18}\text{F}$ ]**8a** shows labeling of  $\beta$ -amyloid plaques associated with blood vessel walls in human brain sections of subjects with CAA and also in the tissue of AD brain sections. The results suggest that [ $^{18}\text{F}$ ]**8a** may be a useful PET imaging agent for selectively detecting  $\text{A}\beta$  plaques associated with cerebral vessels in the living human brain.



## INTRODUCTION

Cerebral amyloid angiopathy (CAA) is a common cause of stroke and dementia in older people. Patients typically present pathological symptoms associated with lobar intracranial macrohemorrhages or microbleeds. Post-mortem studies suggest that there are distinctive morphological changes in the cerebral vessels including the deposition of  $\beta$ -amyloid ( $\text{A}\beta$ ) peptide aggregates, of which  $\text{A}\beta$  peptides are the most common.<sup>1,2</sup> The depositions are located in small to medium-sized cerebral and leptomeningeal arteries and less prominently in the walls of capillaries and veins. Similar to the deposition of  $\text{A}\beta$  in the parenchymal brain tissue in Alzheimer's disease (AD), the  $\text{A}\beta$  peptides form  $\text{A}\beta$  aggregates and neurofibrillary plaques are accumulated in the cerebral blood vessels. As the deposition of  $\text{A}\beta$  aggregates increases with time, they become hardened. These changes in the cerebral blood vessels lead to microbleeds.<sup>3–6</sup> It has been estimated that CAA is present in 55–59% of dementia patients. At least 30% of the dementia patients showed severe CAA, as compared to 7–24% in nondemented patients.<sup>7,8</sup> In general, there is a very close, but not parallel, relationship between CAA and Alzheimer's disease (AD). They also share a set of common genetic risk factors. It is believed that there are specific mechanism(s) which put age-related cerebrovascular degeneration at a critical point in the pathogenesis of AD.<sup>9,10</sup> Evidence collected from post-mortem examination of brain tissues from CAA and AD patients found  $\text{A}\beta$  deposition in the parenchymal and cortical arteries of the brains of AD subjects, while in CAA patients the same deposition was visible predominantly in the blood vessels.<sup>11,12</sup>

Imaging  $\text{A}\beta$  plaques in the brain is generally accepted as a potential useful tool for studying the pathophysiology of neurodegenerative diseases associated with the formation of

$\beta$ -amyloid. One of the leading protocols is [ $^{11}\text{C}$ ]PIB ([ $^{11}\text{C}$ ]1) (Pittsburgh compound B)/PET imaging of  $\text{A}\beta$  plaques in the living brain.<sup>13–16</sup> Recently, several reports on [ $^{11}\text{C}$ ]1/PET imaging in CAA and post-stroke patients suggested that  $\text{A}\beta$  depositions could be detected in the brain tissue as well as in the blood vessels.<sup>6,13,17–19</sup> Because **1** is a small molecule, it readily penetrates the intact blood–brain barrier; therefore, [ $^{11}\text{C}$ ]1/PET images of the  $\text{A}\beta$  deposition represents the map of total  $\text{A}\beta$  deposition in the brain, as well as in the cerebral vessels.

To improve the availability of PET tracers for routine clinical practice, several  $^{18}\text{F}$   $\text{A}\beta$ -plaque imaging agents, including [ $^{18}\text{F}$ ]florbetapir f 18 ([ $^{18}\text{F}$ ]AV-45, [ $^{18}\text{F}$ ]5),<sup>20–24</sup> [ $^{18}\text{F}$ ]florbetaben f 18 ([ $^{18}\text{F}$ ]AV-1, BAY-94–9172, [ $^{18}\text{F}$ ]4),<sup>25–28</sup> [ $^{18}\text{F}$ ]flutemetamol f 18 ([ $^{18}\text{F}$ ]FPIB, GE067, [ $^{18}\text{F}$ ]6)<sup>29–33</sup> and 2-(2-([ $^{18}\text{F}$ ]fluoro)-6-methylaminopyridin-3-yl)benzofuran-5-ol ([ $^{18}\text{F}$ ]AZD4694, [ $^{18}\text{F}$ ]7)<sup>34</sup> have been developed and found to be useful PET agents for targeting  $\text{A}\beta$  plaques in the brain (Figure 1). The phase III clinical trial for [ $^{18}\text{F}$ ]5 has been completed,<sup>24</sup> and this  $\text{A}\beta$ -plaque targeting imaging agent is currently under regulatory review for approval. Similar to [ $^{11}\text{C}$ ]1, [ $^{18}\text{F}$ ]5 labels all  $\text{A}\beta$  plaques, those deposited in the parenchymal of the brain, as well as those in the cerebrovascular vessels. To differentially diagnose the CAA related accumulation of  $\text{A}\beta$  plaques, a [ $^{18}\text{F}$ ] labeled  $\text{A}\beta$ -plaque imaging agent for specifically detecting  $\text{A}\beta$  deposition located on the wall of cerebral blood vessels is needed.

To be able to differentiate between  $\text{A}\beta$  plaques in the brain and those on the wall of cerebrovascular vessels, a series of

Received: July 14, 2011

Published: October 19, 2011

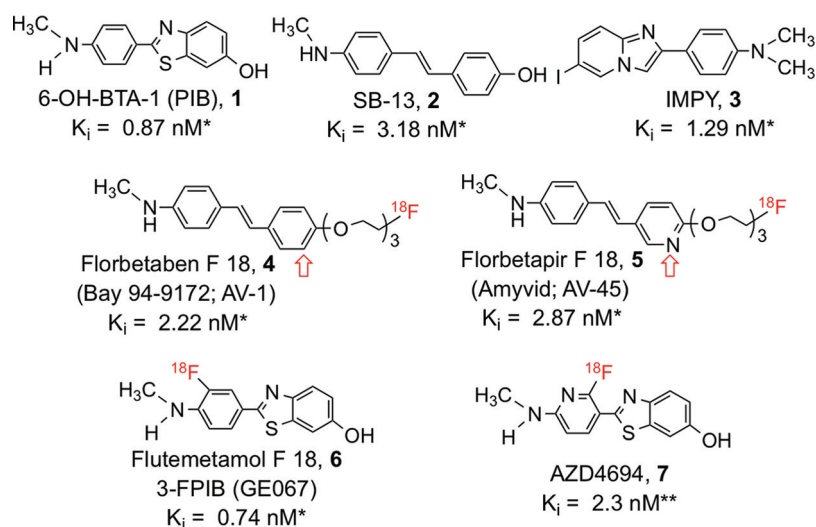


**Figure 1.** The chemical structures and binding affinities of imaging agents targeting  $A\beta$  plaques in the brain are listed. All of these agents are small, neutral molecules showing high binding affinity and the ability to penetrate intact blood–brain barrier in vivo (previously published values  $^*$ ,  $^{22}$   $^{**34}$ ).

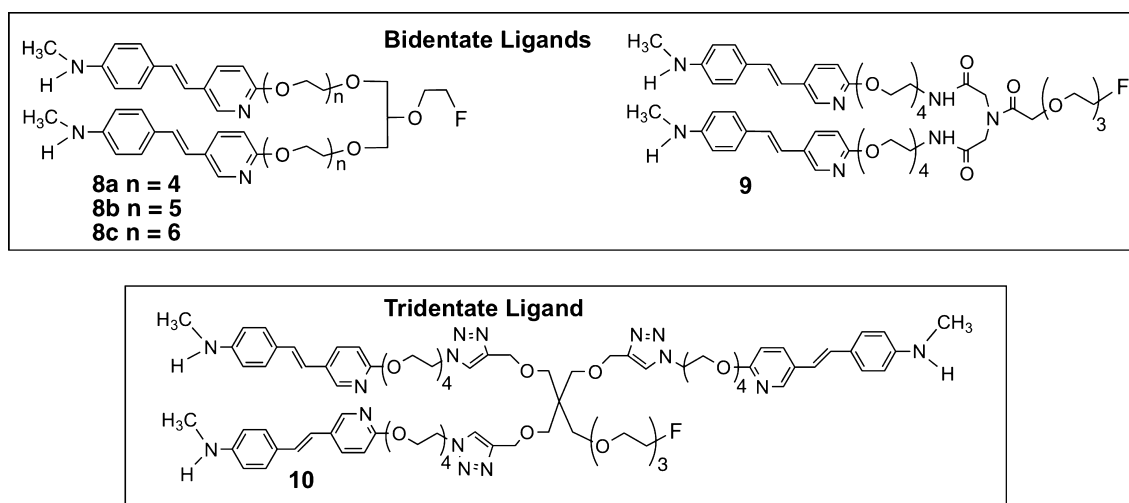


**Figure 2.** Multidentate (bidentate and tridentate) ligands, **8a**, **8b**, **8c**, **9**, and **10**, based on styrylpyridine cores aiming at multiple binding sites within the repeated  $\beta$ -sheet structure are shown. These novel ligands are designed to bind to the  $A\beta$  aggregates via a divalent or a trivalent attachment (binding) sites.

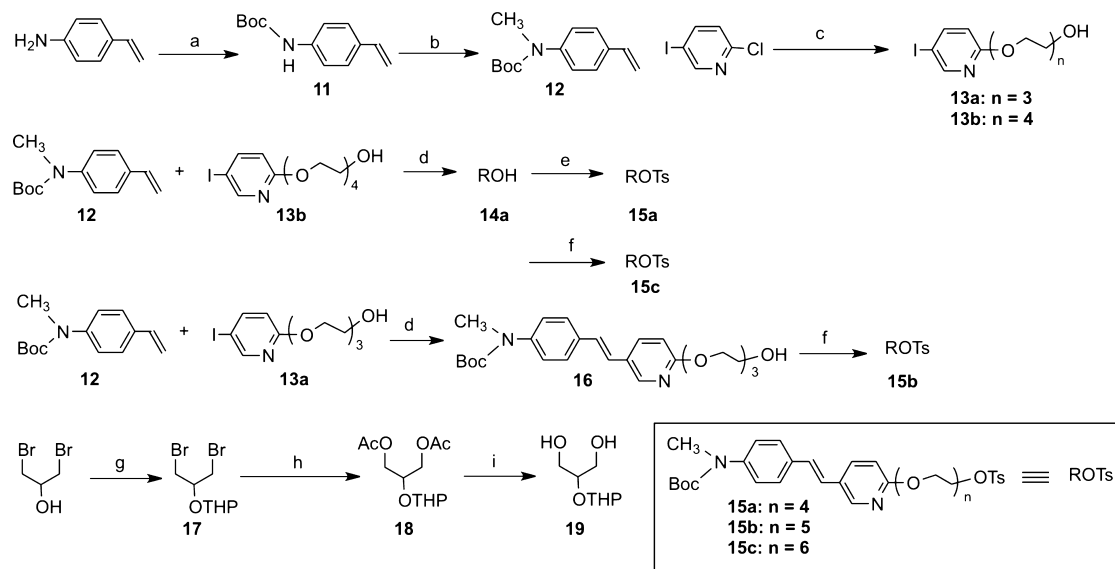
[ $^{18}\text{F}$ ] imaging agents containing two styrylpyridine cores separated by long pegylated chains ( $n > 8$ ) was prepared and tested. We reasoned that the “bivalent or trivalent ligands” containing two or three styrylpyridine binding cores would retain a high binding affinity toward the  $A\beta$  plaques due to the presence of multiple binding sites within the repeated  $\beta$ -sheet structure (Figure 2). It is probable that the multidentate styrylpyridine derivatives with the appropriate spacing between the binding moieties would display good binding to the  $A\beta$  aggregates and that they would be unable to penetrate the intact blood–brain barrier (BBB) in vivo due to their high molecular weights, which exceed 600, a general cutoff point for a simple and neutral molecule to penetrate the BBB by diffusion.<sup>21</sup> Therefore, the “bidentate or tridentate ligands”, **8**, **9**, and **10**, would likely bind only to the  $A\beta$  aggregates located outside of the blood–brain barrier on the vessel walls in CAA patients.

Reported herein is the synthesis and characterization of several  $A\beta$  aggregate-binding ligands, **8a**, **8b**, **8c**, **9**, and **10**, which do not cross the intact blood–brain barrier, and

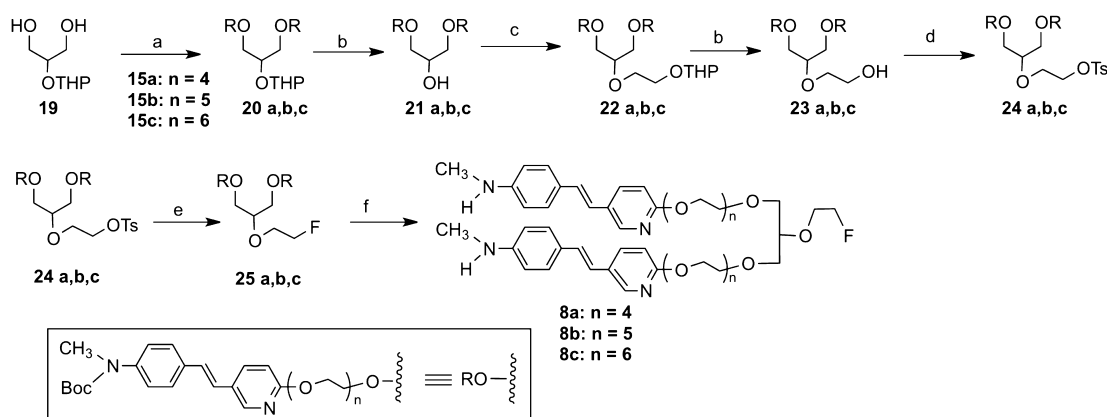
therefore may specifically target  $A\beta$  aggregates located on the cerebrovascular vessel walls outside of the BBB of CAA subjects.

## RESULTS

**Chemical Synthesis of Bivalent and Trivalent Styrylpyridine Derivatives, **8a**, **8b**, **8c**, **9**, and **10**.** The synthesis of the **5** derivatives, **8a**, **8b**, **8c**, **9**, and **10**, with two (bivalent ligand) or three (trivalent ligand) styrylpyridine binding moieties tethered by a polyethylene glycol chain was successfully achieved as described in Schemes 1, 2, 3, and 4. For the first series of bivalent ligands, compound **8**, the binding core, styrylpyridine, was attached with different chain lengths of polyethylene glycol (**8a**, **8b**, **8c**,  $n = 4, 5$ , or  $6$ ). The hydroxyl ends of the polyethylene glycol tethered with styrylpyridines were attached to the 1- and 3-hydroxy positions of a glycerol. The 2-hydroxyl group of the glycerol was linked to an ethylene glycol group, leaving one free hydroxyl group, through which the fluorine atom was end-capped. The molecule has an achiral center and the hydroxyl groups of the glycerol provided a

Scheme 1<sup>a</sup>

<sup>a</sup>Reagents and conditions: (a) (Boc)<sub>2</sub>O, H<sub>2</sub>O, 35 °C; (b) NaH, CH<sub>3</sub>I, DMF, rt; (c) triethylene glycol, CsCO<sub>3</sub>, DMF, 150 °C; (d) K<sub>2</sub>CO<sub>3</sub>, Bu<sub>4</sub>NBr, Pd(OAc)<sub>2</sub>, DMF, 60 °C; (e) TsCl, Et<sub>3</sub>N, DMAP, DCM, rt; (f) diethylene glycol ditosylate, NaH, DMF, rt; (g) DHP, PPTS, EtOH, rt; (h) K<sub>2</sub>CO<sub>3</sub>, Bu<sub>4</sub>NI, Bu<sub>4</sub>NOAc, ACN; (i) NH<sub>3</sub>, CH<sub>3</sub>OH.

Scheme 2<sup>a</sup>

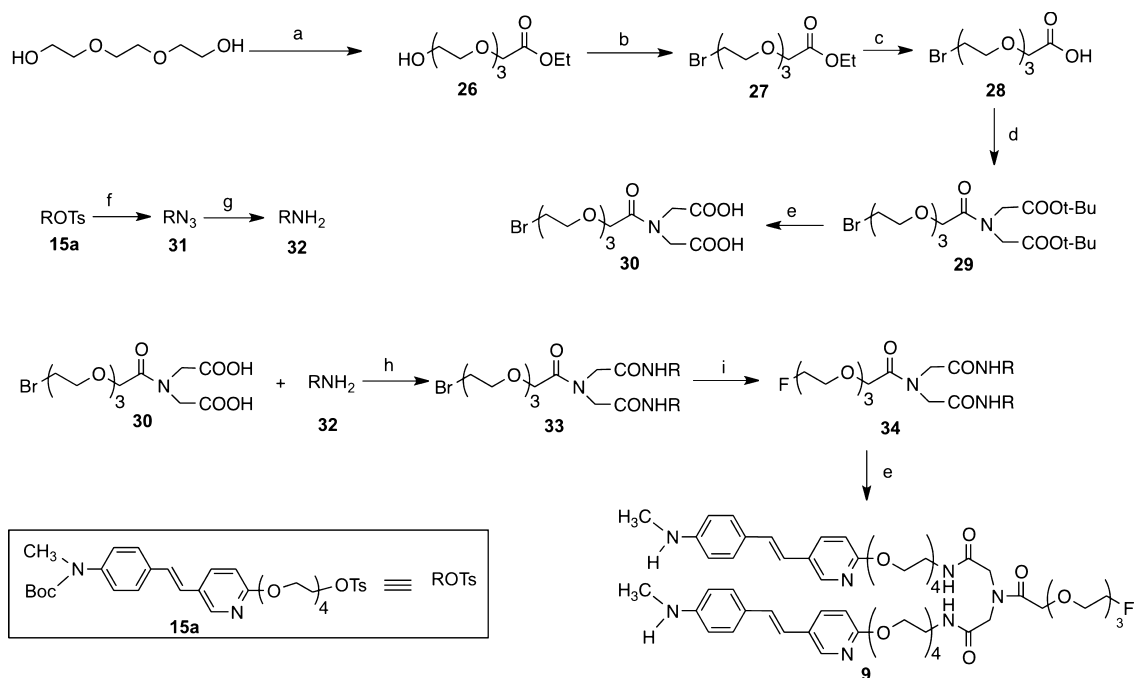
<sup>a</sup>Reagents and conditions: (a) NaH, 2 equiv **15**, DMF, rt; (b) PPTS, EtOH; (c) NaH, 2-(2-bromoethoxy)-tetrahydro-2H-pyran, DMF, rt; (d) TsCl, Et<sub>3</sub>N, DMAP, DCM, rt; (e) TBAF, THP, 70 °C; (f) TFA, rt.

convenient way of stretching between the two styrylpyridine cores with polypegylated chains while leaving one more site for an additional ethylene glycol group for [<sup>18</sup>F] labeling. We chose to use ether linkage (for **8a**, **8b**, **8c**) or amide linkage (for **9**) instead of carboxyl esters, in consideration of in vivo stability. However, the character of the linkage bond, ether vs amide, apparently has a dramatic effect on the in vitro binding affinity to the A $\beta$  plaques, see Discussion below. We also used “click chemistry” to explore the feasibility of constructing a tridentate ligand, **10**, in which three styrylpyridine cores would be included in one single molecule.

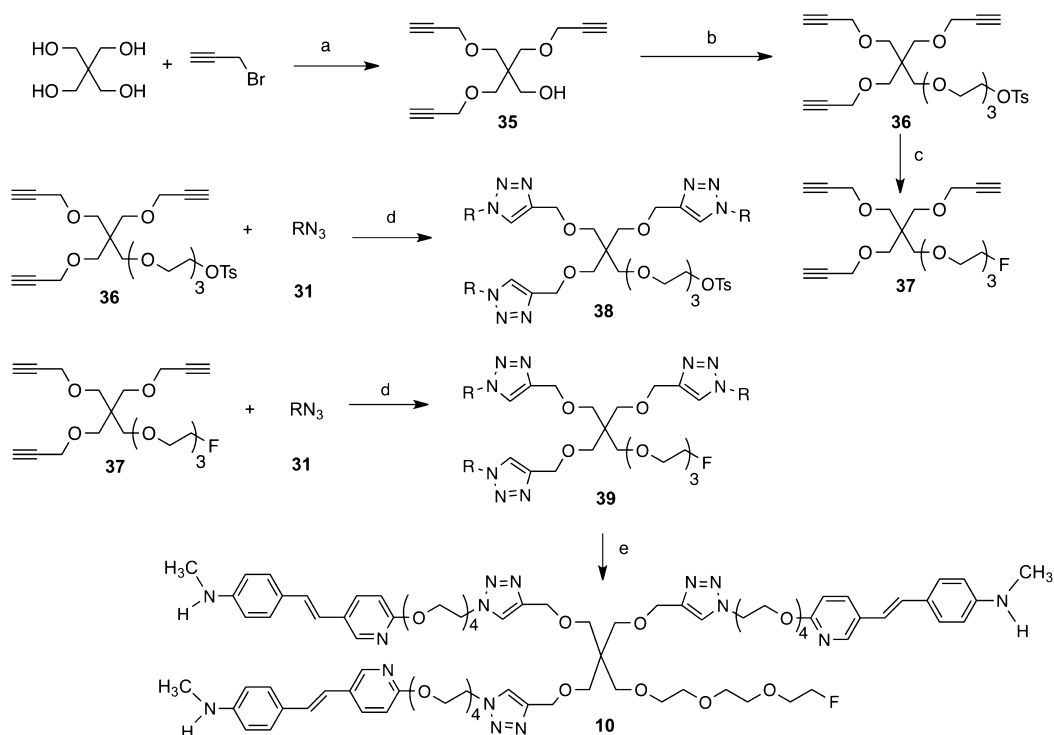
The intermediates **11**–**19**, **26**, and **35** were readily prepared according to similar reported methods.<sup>35–37</sup> Using the Williamson ether synthesis method, dialcohol **19** and tosylates **15** were stitched together (Scheme 1) and the key bivalent intermediates **20a**–**c** were synthesized in good yields. Following a six-step transformation, fluoroethoxy group tethered bivalent styrylpyridine derivatives, **8a**–**c**, were obtained (Scheme 2). For

the synthesis of the other bivalent styrylpyridine derivative, **9**, linked via amide bonds, the key intermediates, amine **32** and diacid **30**, were prepared first, followed by a 1-hydroxybenzotriazole hydrate/*N*-(3-dimethylaminopropyl)-*N*'-ethylcarbodiimide hydrochloride (HOBt/EDCI) promoted coupling reaction. The intermediate **33** was employed as the starting material for fluorination, and subsequently the Boc protection group was removed to give **9** in an acceptable yield.

For preparation of a tridentate ligand, we decided to use pentaerythritol as the backbone structure (Scheme 4). Three of the hydroxyl groups were reacted with propargyl bromide, leaving one hydroxyl group for additional pegylation ( $n = 3$ ). The end of the triglycolated hydroxyl group was capped with a fluorine atom. To assemble the targeted tridentate ligand, **10**, containing three 1,2,3-triazole rings, “click chemistry” between azide and alkyne was carried out. The desired intermediate **37** was first prepared through a simple three-step sequence. At this stage, copper-catalyzed “click chemistry”<sup>38</sup> was utilized to

Scheme 3<sup>a</sup>

<sup>a</sup>Reagents and conditions: (a)  $\text{N}_2\text{CHCO}_2\text{C}_2\text{H}_5$ ,  $\text{BF}_3$ ,  $\text{Et}_2\text{O}$ ,  $\text{DCM}$ ,  $0^\circ\text{C}$ ; (b)  $\text{NBS}$ ,  $\text{PPh}_3$ ,  $\text{DCM}$ ,  $0^\circ\text{C}$ ; (c)  $\text{NaOH}$ ,  $\text{THF}$ ,  $\text{rt}$ ; (d)  $\text{HOBT}$ ,  $\text{EDCI}$ ,  $\text{DIPEA}$ ,  $\text{di-tert-butyl iminodiacetate}$ ,  $\text{DMF}$ ,  $\text{rt}$ ; (e)  $\text{TFA}$ ,  $\text{rt}$ ; (f)  $\text{NaN}_3$ ,  $\text{DMF}$ ,  $60^\circ\text{C}$ ; (g)  $\text{PPh}_3$ ,  $\text{H}_2\text{O}$ ,  $\text{THF}$ ,  $60^\circ\text{C}$ ; (h)  $\text{DCC}$ ,  $\text{DMAP}$ ,  $\text{DCM}$ ,  $\text{rt}$ ; (i)  $\text{TBAF}$ ,  $\text{THF}$ ,  $70^\circ\text{C}$ .

Scheme 4<sup>a</sup>

<sup>a</sup>Reagents and conditions: (a) 40%  $\text{NaOH}$ ,  $\text{DMSO}$ ,  $\text{rt}$ ; (b)  $\text{NaH}$ , triethylene glycol di(*p*-toluenesulfonate),  $\text{DMF}$ ,  $\text{rt}$ ; (c)  $\text{TBAF}$ ,  $\text{THF}$ ,  $70^\circ\text{C}$ ; (d) sodium ascorbate,  $\text{CuSO}_4$ , *t*- $\text{BuOH}$ ,  $\text{H}_2\text{O}$ ,  $\text{rt}$ ; (e)  $\text{TFA}$ ,  $\text{rt}$ .

assemble the styrylpyridine polyethylene glycol-trimerized intermediates **38** and **39**. The final product, trivalent ligand **10**, was obtained by a simple acidic deprotection of intermediate **39**.

Two HPLC conditions were used to test the purity of the final compounds, **8a**, **8b**, **8c**, **9**, and **10**. Using a Phenomenex Luna  $5\ \mu\text{C}18$  250 mm  $\times$  4.60 mm column, eluted with  $\text{ACN}/\text{water}$ , 8/2, 1 min/mL or a Phenomenex Luna  $5\ \mu\text{C}18$

250 mm × 4.60 mm column, eluted with MeOH/water, 9/1, 1 min/mL. All of the final tested samples showed a purity >95%. The HPLC profiles are included in the Supporting Information.

**In Vitro Binding Studies of [<sup>18</sup>F]5 to Aβ-Aggregates in the AD Brain Tissue Homogenates.** An in vitro binding assay was employed to measure the inhibition of [<sup>18</sup>F]5 binding to Aβ-aggregates in the AD brain tissue homogenates (see Supporting Information). Inhibition constants ( $K_i$ , nM) of various agents against the binding of [<sup>18</sup>F]5 to Aβ-aggregates are shown in Table 1. In addition, standard ligands, such as **1**, **4**,

**Table 1. Inhibition Constants ( $K_i$ , nM) of Aβ Plaques Targeting Ligands against Binding of [<sup>18</sup>F]5 to Aβ Plaques in Post-Mortem AD Brain Homogenates<sup>a</sup>**

compd	$K_i$ (nM)	compd	$K_i$ (nM)
PIB, <b>1</b>	0.87 ± 0.18	<b>8a</b> ( $n = 4$ )	3.24 ± 1.92
SB-13, <b>2</b>	3.18 ± 1.04	<b>8b</b> ( $n = 5$ )	7.71 ± 3.56
IMPY, <b>3</b>	1.29 ± 0.46	<b>8c</b> ( $n = 6$ )	3.86 ± 1.05
florbetaben (AV-1), <b>4</b>	2.22 ± 0.54	<b>25a</b>	>1000
florbetapir (AV-45), <b>5</b>	2.87 ± 0.17	<b>9</b> ( $n = 3$ )	71.2 ± 16.8
flutemetamol (3-FPIB), <b>6</b>	0.74 ± 0.38	<b>10</b>	468

<sup>a</sup>Reference 22.

**5**, and **6**, were tested in the same binding assay (see Table 1). As expected, high binding affinities were obtained for the known compounds within the range of <5 nM. The glycerol-based bivalent ligands, **8a**, **8b**, and **8c**, displayed excellent binding affinities ( $K_i = 3.24$ , 7.71, and 3.86 nM, respectively). It appears that the chain length of the pegylation has no effect on the binding affinity. The  $K_i$  values (3–7 nM) were comparable when the chain length was 4, 5, or 6. However, the amide-based bivalent ligand, **9**, showed a significantly lower affinity,  $K_i = 71.2$  nM. The amide linkage is apparently not suitable for designing this series of bivalent ligand. The trivalent ligand, **10**, also displayed a dramatically low binding affinity,  $K_i = 468$  nM.

**Radiolabeling of Bivalent and Trivalent Styrylpyridine Derivatives, [<sup>18</sup>F]8a, 8b, 8c, 9, and 10.** The radiolabeling of the bidentate and tridentate ligands, **8a–c**, **9**, and **10**, was successfully performed using the same protocol as reported for the preparation of [<sup>18</sup>F]5 (see Scheme 5 and Figure 3).<sup>22</sup> The labeling yields (about 30% EOS) were comparable to that observed for [<sup>18</sup>F]5, and the radiochemical purity was >98%.

**Autoradiography of Post-Mortem Brain Tissue Sections with [<sup>18</sup>F]5 and [<sup>18</sup>F]8a.** When confirmed CAA brain sections were incubated with [<sup>18</sup>F]8a, the resulting autoradiogram clearly demonstrated a selective and highly dense labeling of the Aβ plaques of cerebral blood vessels with low labeling in the other areas of the brain sections (see Figure 4, upper panel). The labeling in the CAA brain sections was highly discrete. It is likely that in the CAA brain only the walls of

cerebral blood vessels contained Aβ plaques; therefore the [<sup>18</sup>F]8a only accumulated in these areas. For comparison, AD and healthy control (HC) brain sections were also labeled with [<sup>18</sup>F]5 or [<sup>18</sup>F]8a. As expected, in the AD brain sections, which contained Aβ plaques in both the parenchymal tissue and the blood vessels, the sections were labeled intensely by both tracers. Because of a lack of Aβ plaques, both tracers showed very low labeling in the healthy control (HC) brain sections (Figure 4 lower panel).

To further confirm the nature of the Aβ plaque-labeling of CAA brain sections, a comparison experiment between autoradiography of [<sup>18</sup>F]8a (Figure 5A,B) and fluorescent staining with thioflavin S (Figure 5C,D) was performed using neighboring CAA occipital brain sections. The results clearly indicate that the same labeling of the major blood vessels was observed with thioflavin S as with [<sup>18</sup>F]8a. The data support the conclusion that [<sup>18</sup>F]8a labeled Aβ plaques located on the major blood vessels in the CAA brain (Figure 5).

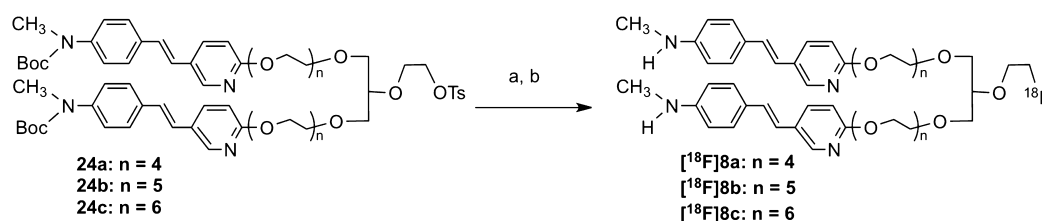
**In Vivo Biodistribution in Mice.** After an iv injection in normal mice, [<sup>18</sup>F]8a, **8b**, and **8c** showed relatively low brain uptake ranging between 0.3 and 0.4% dose/gram at 2 min (Table 2). In comparison to the brain uptake of [<sup>18</sup>F]5, which showed 7.8% dose/gram at 2 min, the bidentate ligands, [<sup>18</sup>F]8a, **8b**, and **8c**, clearly displayed a very low brain penetration. The low brain penetration of these new tracers would enable the selective labeling of Aβ plaques located on the major blood vessels in the CAA brain.

## DISCUSSION

Cerebral amyloid angiopathy (CAA) and Alzheimer's disease (AD) share common risk factors, mainly the accumulation of Aβ aggregates. It is generally believed that the pathology of CAA is associated with the deposit of β-amyloid on the walls of the cortical and leptomeningeal blood vessels. In addition to being a disease-defining pathological marker of AD, Aβ plaques are believed to play a significant role in the pathophysiological mechanisms associated with cerebral amyloid angiopathy. The ability to use PET imaging to determine the location and concentration of Aβ aggregates would be useful for diagnostic purposes.

There are two major prerequisites for imaging agents targeting Aβ plaques associated with cerebral blood vessel walls: (1) High binding affinity to Aβ plaques. To evaluate the feasibility of new ligands targeting the Aβ plaques of cerebral blood vessel walls suitable as CAA imaging agents, we employed an in vitro assay using AD brain tissue homogenates against the binding of [<sup>18</sup>F]5 to measure the binding affinity. (2) Selective labeling of Aβ plaques on cerebral blood vessel walls and not in the cerebral parenchymal tissue: Preliminary testing of this requirement was based on biodistribution (brain uptake at 2 min after an iv injection) of [<sup>18</sup>F] labeled ligands in normal

**Scheme 5<sup>a</sup>**



<sup>a</sup>Reagents and conditions: (a) Na[<sup>18</sup>F]fluoride, K[2,2,2]/K<sub>2</sub>CO<sub>3</sub>; (b) 6N HCl.

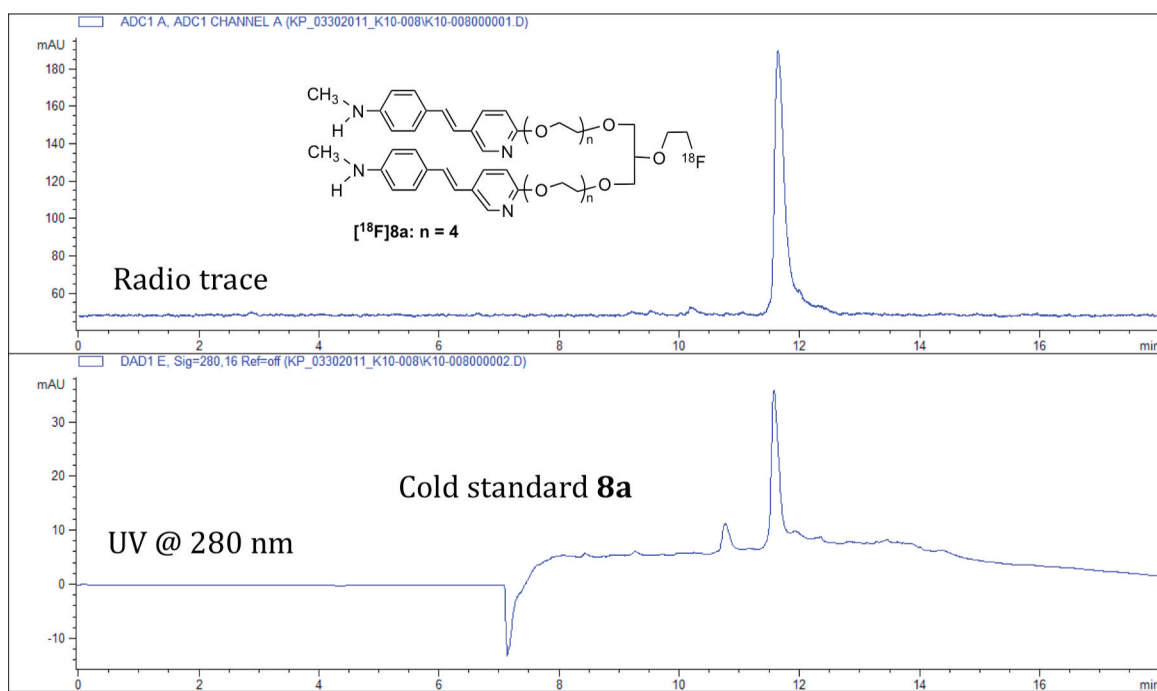


**Figure 3.** HPLC profiles of  $[^{18}\text{F}]\mathbf{8a}$  and coinjected cold standard  $\mathbf{8a}$  on a reversed phase Gemini C18 column (250 mm  $\times$  4.6 mm) with the following gradient and a flow rate of 1 mL/min: 0–2 min 100% ammonium formate buffer (10 mM); 2–5 min ammonium formate buffer 100% to 30%, ACN 0–70%; 5–10 min ammonium formate buffer 30% to 0%, ACN 70–100%; 10–15 min 0–100% ammonium formate buffer, 100% to 0% ACN; 15–18 min 100% ammonium formate buffer.

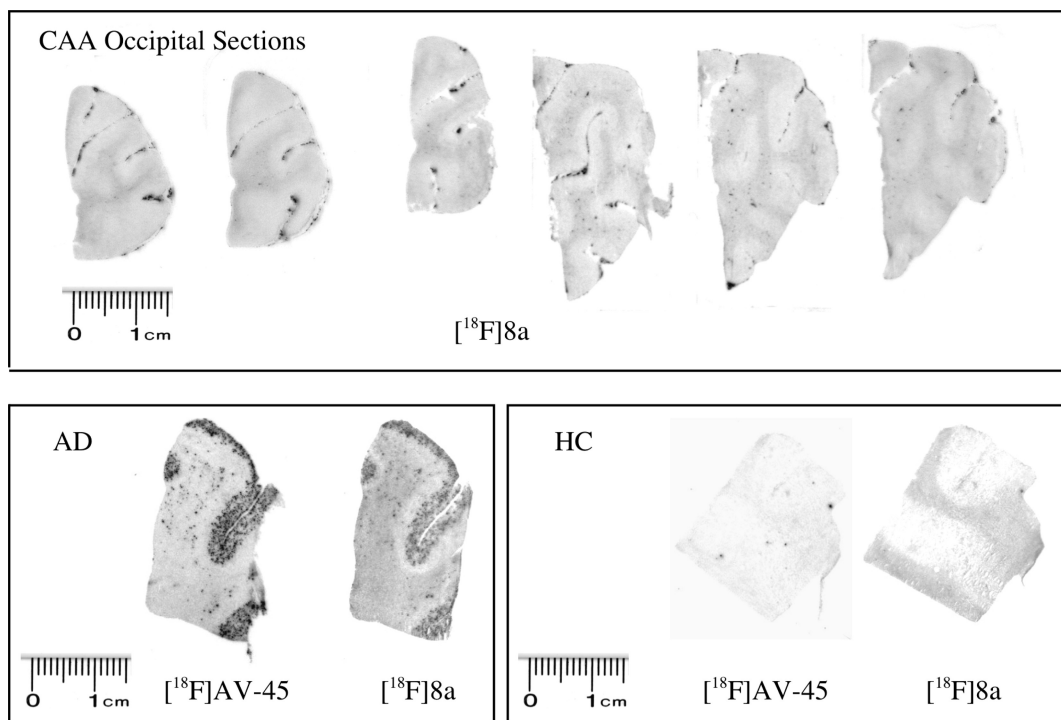


**Figure 4.** In the upper panel the autoradiography of post-mortem human brain sections of occipital samples from cerebral amyloid angiopathy (CAA) using the new bivalent ligand,  $[^{18}\text{F}]\mathbf{8a}$ , showed a highly distinctive labeling at the blood vessels. Other brain parenchymal regions displayed very little labeling, which suggests that there was a selective accumulation of  $A\beta$  plaques in the vessel walls in this CAA patient. The lower panel shows brain sections of AD and healthy control (HC) subjects using either  $[^{18}\text{F}]\text{AV-45}$  ( $[^{18}\text{F}]\mathbf{5}$ ) or  $[^{18}\text{F}]\mathbf{8a}$ . The AD brain section showed highly significant labeling of  $A\beta$  plaques, while both tracers showed little or no binding in the HC sections.

mice. We reasoned that the inability of the new ligands to penetrate the intact blood–brain barrier (BBB) supported the conclusion that they would label only  $A\beta$  plaques on cerebral blood vessel walls, located outside of the BBB. It will be useful in

the future to evaluate the distribution of  $A\beta$  plaque labeling in various transgenic mice reported recently.<sup>1,39,40</sup> One important consideration is the total number of  $A\beta$  plaques on cerebral blood vessel walls, i.e. the  $B_{\text{max}}$  for these new ligands. Because

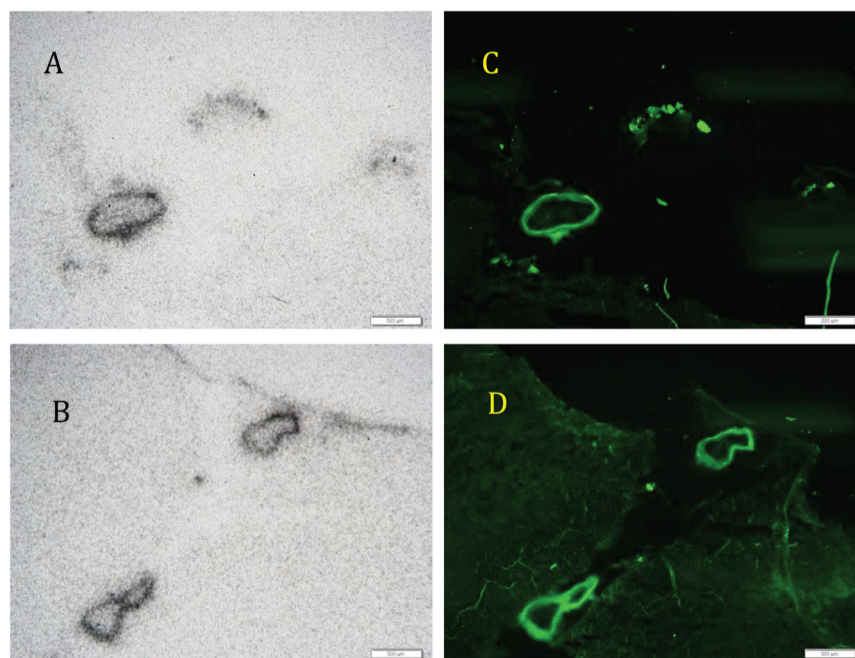


**Figure 5.** Autoradiography of post-mortem human brain samples of cerebral amyloid angiopathy (CAA) using [ $^{18}\text{F}$ ]8a (A,B), which displayed excellent labeling of  $A\beta$  aggregates of the blood vessel walls. There was prominent labeling of major blood vessels only in the CAA brain sections. It is apparent that the parenchymal brain tissue had no  $A\beta$  plaques, therefore no labeling was observed. When the neighboring sections were labeled with thioflavin S (C,D), the fluorescent images displayed a matching staining of blood vessel walls comparable to the images from the autoradiography of [ $^{18}\text{F}$ ]8a. The results strongly suggest that [ $^{18}\text{F}$ ]8a labeled the  $A\beta$  aggregates of the blood vessel walls. The white bars represent a scale of 500  $\mu\text{m}$ .

humans are physically larger and have an increased number of  $A\beta$  plaques on their cerebral blood vessel walls, it may be possible to efficiently detect such differences.

We prepared the desired ligands by stitching together multiple styrylpyridine cores (selective core for binding  $A\beta$  aggregates) using pegylation chains with chain lengths of  $n = 4, 5,$  and  $6$ . It was assumed that  $A\beta$  aggregates composed of parallel  $\beta$ -sheets would likely contain repetitive and neighboring binding sites. These molecules were thus expected to show good binding to  $\beta$ -amyloid and to be excluded from the brain because of their large sizes.

**Table 2. Comparison of the Biodistributions of [ $^{18}\text{F}$ ]8a, [ $^{18}\text{F}$ ]8b, [ $^{18}\text{F}$ ]8c, and [ $^{18}\text{F}$ ]5) in Normal Mice (% dose/g)<sup>a</sup>**

organ	[ $^{18}\text{F}$ ]8a		[ $^{18}\text{F}$ ]5	
	2 min $n = 6$	30 min $n = 6$	2 min* $n = 3$	30 min* $n = 3$
blood	4.77 $\pm$ 1.25	1.54 $\pm$ 0.12	3.14 $\pm$ 0.69	2.80 $\pm$ 0.44
muscle	0.82 $\pm$ 0.16	1.21 $\pm$ 0.15	1.06 $\pm$ 0.39	1.78 $\pm$ 0.34
kidney	8.13 $\pm$ 0.73	9.36 $\pm$ 0.42	10.9 $\pm$ 2.63	6.31 $\pm$ 0.58
liver	21.2 $\pm$ 1.58	21.4 $\pm$ 2.24	21.5 $\pm$ 1.07	12.9 $\pm$ 0.72
<b>brain</b>	<b>0.40 <math>\pm</math> 0.03</b>	<b>0.40 <math>\pm</math> 0.05</b>	<b>7.77 <math>\pm</math> 1.70</b>	<b>1.59 <math>\pm</math> 0.22</b>
bone	1.30 $\pm$ 0.23	2.34 $\pm$ 0.80	1.43 $\pm$ 0.09	1.22 $\pm$ 0.17
organ	[ $^{18}\text{F}$ ]8b		[ $^{18}\text{F}$ ]8c	
	2 min $n = 6$	30 min $n = 6$	2 min $n = 6$	30 min $n = 6$
blood	2.55 $\pm$ 0.21	1.32 $\pm$ 0.04	3.12 $\pm$ 0.17	1.40 $\pm$ 0.10
muscle	1.30 $\pm$ 0.70	1.62 $\pm$ 0.39	0.65 $\pm$ 0.22	1.29 $\pm$ 0.12
kidney	14.9 $\pm$ 0.86	13.4 $\pm$ 1.84	13.7 $\pm$ 2.15	11.7 $\pm$ 0.57
liver	33.5 $\pm$ 6.60	20.0 $\pm$ 6.48	30.2 $\pm$ 3.47	16.0 $\pm$ 1.91
brain	0.40 $\pm$ 0.10	0.34 $\pm$ 0.07	0.29 $\pm$ 0.06	0.38 $\pm$ 0.04
bone	1.64 $\pm$ 0.44	1.80 $\pm$ 0.57	1.06 $\pm$ 0.11	1.36 $\pm$ 0.12

<sup>a</sup>About 925 KBq of each ligand in a saline solution was injected. Mice were sacrificed at 2 and 30 minutes post injection.<sup>22</sup>

Multidentate ligands have been utilized in various biological systems. Dimeric and multimeric ligands targeting  $\alpha_v\beta_3$ -integrin binding sites have been very useful for tumor imaging.<sup>41–47</sup> However, it is likely due to structural limitations of the parallel  $\beta$ -sheets of  $A\beta$  aggregates, as compared to that of the  $\alpha_v\beta_3$ -integrin binding sites, that the structure–activity-relationship for binding would be very different. In this report, we have prepared and examined the multidentate  $A\beta$  aggregate-binding affinity of 8a, 8b, 8c, 9, and 10. Surprisingly, only the bidentate ligands 8a, 8b, and 8c showed the desired high binding affinity comparable to that of [ $^{18}\text{F}$ ]5. The structural difference between the bidentate ligands 8a–c and 9 was the linkage for the pegylated styrylpyridines, i.e. ether vs amide linkage, which may have caused the big difference in binding affinity ( $K_i = 3\text{--}7\text{ nM}$  vs 71 nM). The binding affinity of the tridentate ligand, 10, also showed a dramatic reduction ( $K_i = 468\text{ nM}$ ). This decrease may have been caused by changes in the geometry of the new ligand. These observations suggest that there are space limitations for multidentate ligands to insert themselves into  $\beta$ -amyloid and to bind to neighboring target sites.

The initial data from in vitro labeling of human brain sections also show that similar to [ $^{18}\text{F}$ ]5, [ $^{18}\text{F}$ ]8a is capable of labeling  $A\beta$  aggregates in human AD brain sections (Figure 4). It is important to note that the in vitro autoradiography of confirmed CAA brain sections showed successful labeling of major blood vessels by [ $^{18}\text{F}$ ]8a and the labeling was confirmed by costaining with thioflavin S (Figure 5). The results strongly suggest that it will be feasible to use [ $^{18}\text{F}$ ]8a in imaging the accumulation of  $A\beta$  aggregates on the walls of major cerebral blood vessels in CAA patients. A buildup of  $A\beta$  aggregates in cerebral blood vessels also occurs in patients at risk of stroke and Alzheimer's disease.<sup>19</sup> CAA discriminating  $A\beta$  imaging agents, due to the location of  $A\beta$  aggregates on the wall of cerebral blood vessels,

may provide selective diagnostic tools that would be useful in teasing out the accumulation of A $\beta$  aggregates in different areas, which can be associated with different clinical manifestations. Currently, it is assumed that the A $\beta$  aggregates on the walls of major cerebral blood vessels in CAA are similar to those A $\beta$  plaques in the brain (parenchymal). The new bidentate ligand, [ $^{18}\text{F}$ ]**8a**, will likely bind to A $\beta$  aggregates on the blood vessels in a similar binding mechanism as it would bind to A $\beta$  plaques in the brain. Further studies will be required to confirm that this assumption is true.

One other key factor for consideration is the number of binding sites associated with A $\beta$  plaques on the blood vessels walls. These may not be as high as those reported for AD brain  $K_d = 3.72 \pm 0.30$  nM,  $B_{\text{max}} = 8811 \pm 1643$  fmol/mg protein.<sup>22</sup> However, the A $\beta$  plaques located in the blood vessels may be more accessible and readily exposed to the CAA binding agent in the blood circulation. Therefore, the A $\beta$  plaques in CAA may show higher apparent binding sites. This is a critical factor that warrants further investigation.

## CONCLUSION

In summary, multidentate binding ligands targeting A $\beta$  aggregates on cerebral vessels have been prepared and tested. They may provide useful tools for selective diagnosis of cerebral amyloid angiopathy (CAA), a significant risk factor in the older patient population.

## EXPERIMENTAL SECTION

**1. General.** All reagents used for chemical synthesis were commercial products and were used without further purification. CD-1 mice (20–26 g) were used for the biodistribution studies. All protocols requiring the utilization of mice were reviewed and approved by the Institutional Animal Care and Use Committee (University of Pennsylvania and University of the Sciences in Philadelphia). Post-mortem human samples were obtained from phase III clinical trials of [ $^{18}\text{F}$ ]**5**. The synthesis of precursors and bidentate and tridentate styrylpyridine derivatives, **8a**, **8b**, **8c**, **9**, and **10**, was accomplished by the following schemes (Schemes 1–4).

**2-(2-Fluoroethoxy)-1,3-di((E)-2-(2-(2-(5-(4-(methylamino)styryl)pyridin-2-yloxy)ethoxy)ethoxy)ethoxy)propane (8a).** A solution of **25a** (0.0338 g, 0.031 mmol) in 0.9 mL of trifluoroacetic acid (TFA) and 0.1 mL of dimethyl sulfide was stirred at rt for 1 h. The reaction mixture was evaporated in vacuo, and the residue was purified by FC (DCM/MeOH = 92.5/7.5) to give 0.024 g yellowish oil **8a** (yield: 87%).  $^1\text{H}$  NMR (200 MHz,  $\text{CDCl}_3$ )  $\delta$ : 8.14 (d, 2H,  $J = 2.2$  Hz), 7.76 (dd, 2H,  $J = 2.4$  Hz,  $J = 8.8$  Hz), 7.35 (d, 4H,  $J = 8.4$  Hz), 6.86 (d, 4H,  $J = 8.0$  Hz), 6.77 (d, 2H,  $J = 8.6$  Hz), 6.60 (d, 4H,  $J = 8.6$  Hz), 4.65 (t, 1H,  $J = 4.2$  Hz), 4.49 (t, 4H,  $J = 4.8$  Hz), 4.41 (t, 1H,  $J = 4.2$  Hz), 3.78–3.97 (m, 6H), 3.63–3.74 (m, 25H), 3.55–3.59 (m, 4H), 2.88 (s, 6H).  $^{13}\text{C}$  NMR (200 MHz,  $\text{CDCl}_3$ )  $\delta$ : 162.9, 149.3, 145.2, 135.3, 128.6, 127.8, 126.8, 120.7, 112.7, 111.5, 85.2, 81.8, 79.0, 71.82, 71.14, 70.9, 70.9, 70.8, 70.2, 70.0, 69.8, 65.5, 30.9. HRMS (ESI) calculated for  $\text{C}_{49}\text{H}_{68}\text{FN}_4\text{O}_{11}$  ( $\text{MH}^+$ ), 907.4869; found, 907.4870.

**2-(2-Fluoroethoxy)-1,3-di((E)-2-(2-(2-(5-(4-(methylamino)styryl)pyridin-2-yloxy)ethoxy)ethoxy)ethoxy)propane (8b).** Compound **8b** was prepared from **25b** (0.0650 g, 0.054 mmol) in 0.5 mL of TFA and 0.05 mL of dimethyl sulfide, with the same procedure described for compound **8a**. Compound **8b**: 0.050 g (yield: 93%).  $^1\text{H}$  NMR (200 MHz,  $\text{CDCl}_3$ )  $\delta$ : 8.14 (d, 2H,  $J = 2.2$  Hz), 7.75 (dd, 2H,  $J = 2.4$  Hz,  $J = 8.6$  Hz), 7.34 (d, 4H,  $J = 8.6$  Hz), 6.86 (d, 4H,  $J = 8.0$  Hz), 6.76 (d, 2H,  $J = 8.6$  Hz), 6.59 (d, 4H,  $J = 8.6$  Hz), 4.65 (t, 1H,  $J = 4.3$  Hz), 4.48 (t, 4H,  $J = 4.8$  Hz), 4.41 (t, 1H,  $J = 4.3$  Hz), 3.80–3.96 (m, 6H), 3.52–3.77 (m, 37H), 2.86 (s, 6H).  $^{13}\text{C}$  NMR (200 MHz,  $\text{CDCl}_3$ )  $\delta$ : 162.8, 149.2, 145.2, 135.3, 128.5, 127.8, 126.7, 120.6, 112.7, 111.4, 85.1, 81.8, 78.9, 71.8, 71.1, 70.8, 70.7, 70.2, 70.0, 69.8, 65.4, 30.8. HRMS (ESI) calculated for  $\text{C}_{53}\text{H}_{76}\text{FN}_4\text{O}_{13}$  ( $\text{MH}^+$ ), 995.5393; found, 995.5371.

**2-(2-Fluoroethoxy)-1,3-di((E)-2-(2-(2-(5-(4-(methylamino)styryl)pyridin-2-yloxy)ethoxy)ethoxy)ethoxy)propane (8c).** Compound **8c** was prepared from **25c** (0.0950 g, 0.074 mmol) in 0.9 mL of TFA and 0.1 mL of dimethyl sulfide, with the same procedure described for compound **8a**. Compound **8c**: 0.074 g (yield: 92%).  $^1\text{H}$  NMR (200 MHz,  $\text{CDCl}_3$ )  $\delta$ : 8.13 (d, 2H,  $J = 2.2$  Hz), 7.75 (dd, 2H,  $J = 2.4$  Hz,  $J = 8.6$  Hz), 7.34 (d, 4H,  $J = 8.6$  Hz), 6.85 (d, 4H,  $J = 8.0$  Hz), 6.76 (d, 2H,  $J = 8.6$  Hz), 6.58 (d, 4H,  $J = 8.6$  Hz), 4.64 (t, 1H,  $J = 4.3$  Hz), 4.47 (t, 4H,  $J = 4.8$  Hz), 4.40 (t, 1H,  $J = 4.2$  Hz), 3.81–3.96 (m, 6H), 3.54–3.79 (m, 45H), 2.85 (s, 6H).  $^{13}\text{C}$  NMR (200 MHz,  $\text{CDCl}_3$ )  $\delta$ : 162.7, 149.2, 145.1, 135.2, 128.5, 127.7, 126.6, 120.5, 112.6, 111.4, 85.1, 81.7, 78.8, 71.7, 71.0, 70.8, 70.2, 69.9, 69.8, 65.4, 30.9. HRMS (ESI) calculated for  $\text{C}_{57}\text{H}_{84}\text{FN}_4\text{O}_{15}$  ( $\text{M} + \text{H}^+$ ), 1083.5917; found, 1083.5890.

**2-(2-(2-(2-Fluoroethoxy)ethoxy)ethoxy)-N,N-bis(14-(5-((E)-4-(methylamino)styryl)pyridin-2-yloxy)-2-oxo-6,9,12-trioxa-3-azatetradecyl)acetamide (9).** A solution of **34** (0.0400 g, 0.031 mmol) in 0.9 mL of TFA and 0.1 mL of dimethyl sulfide was stirred at rt for 1 h. The reaction mixture was evaporated in vacuo, and the residue was purified by FC (DCM/MeOH = 92.5/7.5) to give 0.021 g yellowish oil **8a** (yield: 62%).  $^1\text{H}$  NMR (200 MHz,  $\text{CDCl}_3$ )  $\delta$ : 8.14 (d, 2H,  $J = 2.2$  Hz), 7.76 (dd, 2H,  $J = 2.4$  Hz,  $J = 8.6$  Hz), 7.35 (d, 4H,  $J = 8.4$  Hz), 6.86 (d, 4H,  $J = 8.8$  Hz), 6.76 (d, 2H,  $J = 7.2$  Hz), 6.60 (d, 4H, 8.6 Hz), 4.68 (t, 1H,  $J = 4.2$  Hz), 4.42–4.51 (m, 5H), 4.17 (s, 2H), 4.12 (s, 2H), 3.97 (s, 2H), 3.79–3.88 (m, 6H), 3.54–3.70 (m, 28H), 3.43–3.50 (m, 4H), 2.87 (s, 6H).  $^{13}\text{C}$  NMR (200 MHz,  $\text{CDCl}_3$ )  $\delta$ : 170.7, 169.3, 169.1, 162.7, 149.3, 145.2, 135.4, 128.6, 127.8, 126.7, 120.5, 112.7, 111.4, 85.0, 81.7, 70.9, 70.8, 70.6, 70.5, 70.0, 69.6, 65.4, 39.6, 30.9. HRMS (ESI) calculated for  $\text{C}_{56}\text{H}_{79}\text{FN}_7\text{O}_{14}$  ( $\text{M} + \text{H}^+$ ), 1092.5669; found, 1092.5557.

**1,3-Di((E)-1-(2-(2-(2-(2-(5-(4-(methylamino)styryl)pyridin-2-yloxy)ethoxy)ethoxy)ethyl)-1H-1,2,3-triazol-4-yl)methoxy-2-((E)-1-(2-(2-(2-(2-(5-(4-(methylamino)styryl)pyridin-2-yloxy)ethoxy)ethoxy)ethoxy)ethyl)-1H-1,2,3-triazol-4-yl)methoxy)methyl)propane (10).** A solution of **39** (0.0900 mg, 0.046 mmol) in 0.6 mL of TFA and 0.06 mL of dimethyl sulfide was stirred at rt for 1 h. The reaction mixture was evaporated in vacuo, and the residue was purified by FC (DCM/MeOH = 95/5) to give 0.063 g yellowish oil **8a** (yield: 82%).  $^1\text{H}$  NMR (200 MHz,  $\text{CDCl}_3$ )  $\delta$ : 8.12 (d, 3H,  $J = 2.2$  Hz), 7.69–7.76 (m, 6H), 7.33 (d, 6H,  $J = 8.6$  Hz), 6.84 (d, 6H,  $J = 8.6$  Hz), 6.73 (d, 3H,  $J = 8.6$  Hz), 6.58 (d, 6H,  $J = 8.6$  Hz), 4.64 (t, 1H,  $J = 4.2$  Hz), 4.38–4.58 (m, 19H), 3.75–3.88 (m, 13H), 3.42–3.72 (m, 41H), 2.84 (s, 9H).  $^{13}\text{C}$  NMR (200 MHz,  $\text{CDCl}_3$ )  $\delta$ : 162.7, 149.2, 145.4, 145.1, 135.3, 128.5, 127.8, 126.7, 123.7, 120.4, 112.6, 111.3, 85.0, 81.6, 71.2, 71.0, 70.8, 70.8, 70.7, 70.5, 70.3, 69.9, 69.6, 69.5, 65.3, 65.2, 50.3, 45.6, 30.8. HRMS (ESI) calculated for  $\text{C}_{86}\text{H}_{116}\text{FN}_{15}\text{O}_{18}\text{Na}$  ( $\text{M} + \text{Na}^+$ ), 1688.8505; found, 1688.8490.

**tert-Butyl 4-Vinylphenylcarbamate (11).** To a solution of aminostyrene (1.19 g, 10 mmol) in 10 mL of water ( $\text{H}_2\text{O}$ ) was added di-tert-butyl dicarbonate ( $\text{Boc}_2\text{O}$ , 2.40 g, 11 mmol). After vigorously stirring at 35 °C for 4 h, the mixture was extracted with dichloromethane (DCM, 25 mL  $\times$  2). The organic layer was dried by anhydrous sodium sulfate ( $\text{Na}_2\text{SO}_4$ ) and filtered. The filtrate was concentrated, and the residue was purified by flash chromatography (FC) (ethyl acetate (EtOAc)/hexane = 2/8) to give 2.18 g white solid **11** (yield: 99%).  $^1\text{H}$  NMR (200 MHz,  $\text{CDCl}_3$ )  $\delta$ : 7.34 (s, 4H), 6.67 (dd, 1H,  $J = 10.8$  Hz,  $J = 17.6$  Hz), 6.47 (br, 1H), 5.66 (d, 1H,  $J = 17.6$  Hz), 5.17 (d, 1H,  $J = 11$  Hz), 1.53 (s, 9H).

**tert-Butyl Methyl(4-vinylphenyl)carbamate (12).** To a suspension of NaH (60%, 0.600 g, 15 mmol) in 30 mL of *N,N*-dimethylformamide (DMF) was slowly added **11** (2.19 g, 10 mmol) in 20 mL of DMF followed by iodomethane ( $\text{CH}_3\text{I}$ , 7.10 g, 50 mmol). After stirring at room temperature (rt) for 6 h, the reaction mixture was quenched with 40 mL satd ammonium chloride ( $\text{NH}_4\text{Cl}$ ) at 0 °C. The mixture was then extracted with 120 mL of EtOAc. The organic layer was washed with  $\text{H}_2\text{O}$  (40 mL  $\times$  2) as well as brine (40 mL), dried by  $\text{Na}_2\text{SO}_4$ , and filtered. The filtrate was concentrated, and the residue was purified by FC (EtOAc/hexane = 2/8) to give 2.32 g white solid **12** (yield: 99%).  $^1\text{H}$  NMR (200 MHz,  $\text{CDCl}_3$ )  $\delta$ : 7.37 (d, 2H,  $J = 8.6$  Hz), 7.20 (d, 2H,  $J = 8.6$  Hz), 6.70 (dd, 1H,  $J = 11$  Hz,



2-(1,3-Di((E)-2-(2-(2-(2-(5-(4-(tert-butoxycarbonyl(methylamino)styryl)pyridin-2-yloxy)ethoxy)ethoxy)ethoxy)ethoxy)propan-2-yloxy)tetrahydro-2H-pyran (**20b**). Compound **20b** was prepared from NaH (60% in mineral oil, 0.052 g, 1.3 mmol), **19** (0.0581 g, 0.33 mmol), and **15b** (0.469 g, 0.67 mmol) in 8 mL of DMF, with the same procedure described for compound **20a**. Compound **20b**: 0.310 g (yield: 76%). <sup>1</sup>H NMR (200 MHz, CDCl<sub>3</sub>) δ: 8.19 (d, 2H, J = 2.4 Hz), 7.80 (dd, 2H, J = 2.4 Hz, J = 8.6 Hz), 7.45 (d, 4H, J = 8.4 Hz), 7.23 (d, 4H, J = 8.4 Hz), 6.97 (s, 4H), 6.80 (d, 2H, J = 8.6 Hz), 4.79–4.81 (m, 1H), 4.50 (t, 4H, J = 4.8 Hz), 3.84–4.05 (m, 6H), 3.62–3.71 (m, 37H), 3.28 (s, 6H), 1.56–1.96 (m, 6H), 1.47 (s, 18H).

2-(1,3-Di((E)-2-(2-(2-(2-(5-(4-(tert-butoxycarbonyl(methylamino)styryl)pyridin-2-yloxy)ethoxy)ethoxy)ethoxy)ethoxy)ethoxy)propan-2-yloxy)tetrahydro-2H-pyran (**20c**). Compound **20c** was prepared from NaH (60% in mineral oil, 0.080 g, 2 mmol), **19** (0.0851 g, 0.48 mmol), and **15c** (0.745 g, 1 mmol) in 10 mL of DMF, with the same procedure described for compound **20a**. Compound **20c**: 0.522 g (yield: 82%). <sup>1</sup>H NMR (200 MHz, CDCl<sub>3</sub>) δ: 8.19 (d, 2H, J = 2.4 Hz), 7.80 (dd, 2H, J = 2.4 Hz, J = 8.6 Hz), 7.45 (d, 4H, J = 8.4 Hz), 7.23 (d, 4H, J = 8.6 Hz), 6.97 (s, 4H), 6.80 (d, 2H, J = 8.6 Hz), 4.79–4.81 (m, 1H), 4.50 (t, 4H, J = 4.8 Hz), 3.85–4.05 (m, 6H), 3.45–3.71 (m, 45H), 3.28 (s, 6H), 1.56–1.96 (m, 6H), 1.47 (s, 18H).

1,3-Di((E)-2-(2-(2-(2-(5-(4-(tert-butoxycarbonyl(methylamino)styryl)pyridin-2-yloxy)ethoxy)ethoxy)ethoxy)ethoxy)ethoxy)propan-2-ol (**21a**). A mixture of **20a** (0.841 g, 0.73 mmol) and PPTS (0.0183 g, 0.073 mmol) in 7 mL of EtOH was stirred at 55 °C for 3 h. The mixture was concentrated, and the residue was purified by FC (EtOAc/MeOH = 9/1) to give 0.732 g colorless oil **21a** (yield: 94%). <sup>1</sup>H NMR (200 MHz, CDCl<sub>3</sub>) δ: 8.19 (d, 2H, J = 2.4 Hz), 7.80 (dd, 2H, J = 2.4 Hz, J = 8.6 Hz), 7.45 (d, 4H, J = 8.4 Hz), 7.23 (d, 4H, J = 8.6 Hz), 6.97 (s, 4H), 6.80 (d, 2H, J = 8.6 Hz), 4.50 (t, 4H, J = 4.8 Hz), 3.84–4.05 (m, 6H), 3.45–3.80 (m, 28H), 3.28 (s, 6H), 1.47 (s, 18H).

1,3-Di((E)-2-(2-(2-(2-(5-(4-(tert-butoxycarbonyl(methylamino)styryl)pyridin-2-yloxy)ethoxy)ethoxy)ethoxy)ethoxy)ethoxy)propan-2-ol (**21b**). Compound **21b** was prepared from **20b** (0.295 g, 0.24 mmol) and PPTS (0.0060 g, 0.024 mmol) in 3 mL of EtOH, with the same procedure described for compound **21a**. Compound **21b**: 0.177 g (yield: 62%). <sup>1</sup>H NMR (200 MHz, CDCl<sub>3</sub>) δ: 8.19 (d, 2H, J = 2.4 Hz), 7.80 (dd, 2H, J = 2.4 Hz, J = 8.6 Hz), 7.45 (d, 4H, J = 8.4 Hz), 7.23 (d, 4H, J = 8.4 Hz), 6.97 (s, 4H), 6.80 (d, 2H, J = 8.6 Hz), 4.48–4.52 (m, 4H), 3.84–4.05 (m, 6H), 3.45–3.80 (m, 36H), 3.28 (s, 6H), 1.47 (s, 18H).

1,3-Di((E)-2-(2-(2-(2-(5-(4-(tert-butoxycarbonyl(methylamino)styryl)pyridin-2-yloxy)ethoxy)ethoxy)ethoxy)ethoxy)ethoxy)propan-2-ol (**21c**). Compound **21b** was prepared from **20c** (0.524 g, 0.4 mmol) and PPTS (0.0100 g, 0.04 mmol) in 4 mL of EtOH, with the same procedure described for compound **21a**. Compound **21c**: 0.340 g (yield: 69%). <sup>1</sup>H NMR (200 MHz, CDCl<sub>3</sub>) δ: 8.19 (d, 2H, J = 2.4 Hz), 7.80 (dd, 2H, J = 2.4 Hz, J = 8.6 Hz), 7.45 (d, 4H, J = 8.4 Hz), 7.23 (d, 4H, J = 8.4 Hz), 6.97 (s, 4H), 6.80 (d, 2H, J = 8.6 Hz), 4.50 (t, 4H, J = 4.8 Hz), 3.84–4.05 (m, 6H), 3.45–3.80 (m, 44H), 3.28 (s, 6H), 1.47 (s, 18H).

2-(2-(1,3-Di((E)-2-(2-(2-(2-(5-(4-(tert-butoxycarbonyl(methylamino)styryl)pyridin-2-yloxy)ethoxy)ethoxy)ethoxy)ethoxy)ethoxy)propan-2-yloxy)ethoxy)tetrahydro-2H-pyran (**22a**). NaH (60% in mineral oil, 0.0552 g, 1.38 mmol) was placed in a two-neck flask and washed with hexane. Four mL of DMF was added to form a suspension. A solution of **21a** (0.73 g, 0.69 mmol) in 3 mL of DMF was added dropwise at 0 °C. After stirring at rt for 30 min, the mixture was cooled to 0 °C, and a solution of 2-(2-bromoethoxy)tetrahydro-2H-pyran (0.288 g, 1.38 mmol) in 3 mL DMF was added dropwise. The reaction mixture was stirred at rt overnight. The mixture was then poured into 50 mL of cold satd NH<sub>4</sub>Cl and extracted with DCM (30 mL × 2). The organic layer was washed with H<sub>2</sub>O (20 mL) and brine (20 mL), dried over Na<sub>2</sub>SO<sub>4</sub>, concentrated, and purified by FC (EtOAc/MeOH = 98/2) to give 0.574 g of a colorless oil **22a** (yield: 70%). <sup>1</sup>H NMR (200 MHz, CDCl<sub>3</sub>) δ: 8.19 (d, 2H, J = 2.0 Hz), 7.80 (dd, 2H, J = 2.4 Hz, J = 8.6 Hz), 7.45 (d, 4H, J = 8.4 Hz), 7.23 (d, 4H,

J = 8.4 Hz), 6.97 (s, 4H), 6.80 (d, 2H, J = 8.6 Hz), 4.62–4.65 (m, 1H), 4.50 (t, 4H, J = 4.8 Hz), 3.55–3.89 (m, 39H), 3.28 (s, 6H), 1.56–1.96 (m, 6H), 1.47 (s, 18H).

2-(2-(1,3-Di((E)-2-(2-(2-(2-(5-(4-(tert-butoxycarbonyl(methylamino)styryl)pyridin-2-yloxy)ethoxy)ethoxy)ethoxy)ethoxy)ethoxy)propan-2-yloxy)ethoxy)tetrahydro-2H-pyran (**22b**). Compound **22b** was prepared from NaH (60% in mineral oil, 0.0180 g, 0.45 mmol), **21b** (0.172 g, 0.15 mmol), and 2-(2-bromoethoxy)tetrahydro-2H-pyran (0.0627 g, 0.3 mmol) in 2.5 mL of DMF, with the same procedure described for compound **22a**. Compound **22b**: 0.130 g (yield: 68%). <sup>1</sup>H NMR (200 MHz, CDCl<sub>3</sub>) δ: 8.19 (d, 2H, J = 2.4 Hz), 7.80 (dd, 2H, J = 2.4 Hz, J = 8.6 Hz), 7.45 (d, 4H, J = 8.4 Hz), 7.23 (d, 4H, J = 8.4 Hz), 6.97 (s, 4H), 6.80 (d, 2H, J = 8.6 Hz), 4.62–4.65 (m, 1H), 4.50 (t, 4H, J = 4.8 Hz), 3.52–3.89 (m, 47H), 3.28 (s, 6H), 1.56–1.96 (m, 6H), 1.47 (s, 18H).

2-(2-(1,3-Di((E)-2-(2-(2-(2-(5-(4-(tert-butoxycarbonyl(methylamino)styryl)pyridin-2-yloxy)ethoxy)ethoxy)ethoxy)ethoxy)ethoxy)propan-2-yloxy)ethoxy)tetrahydro-2H-pyran (**22c**). Compound **22c** was prepared from NaH (60% in mineral oil, 0.022 g, 0.55 mmol), **21c** (0.333 g, 0.27 mmol), and 2-(2-bromoethoxy)tetrahydro-2H-pyran (0.115 g, 0.55 mmol) in 4 mL of DMF, with the same procedure described for compound **22a**. Compound **22c**: 0.310 g (yield: 83%). <sup>1</sup>H NMR (200 MHz, CDCl<sub>3</sub>) δ: 8.19 (d, 2H, J = 2.4 Hz), 7.80 (dd, 2H, J = 2.4 Hz, J = 8.6 Hz), 7.45 (d, 4H, J = 8.4 Hz), 7.23 (d, 4H, J = 8.4 Hz), 6.97 (s, 4H), 6.80 (d, 2H, J = 8.6 Hz), 4.62–4.65 (m, 1H), 4.50 (t, 4H, J = 4.8 Hz), 3.57–3.89 (m, 55H), 3.28 (s, 6H), 1.56–1.96 (m, 6H), 1.47 (s, 18H).

2-(1,3-Di((E)-2-(2-(2-(2-(5-(4-(tert-butoxycarbonyl(methylamino)styryl)pyridin-2-yloxy)ethoxy)ethoxy)ethoxy)ethoxy)ethoxy)propan-2-yloxy)ethanol (**23a**). A mixture of **22a** (0.570 g, 0.48 mmol) and PPTS (0.0120 g, 0.048 mmol) in 6 mL of EtOH was stirred at 55 °C for 6 h. The mixture was concentrated, and the residue was purified by FC (EtOAc/MeOH = 9/1) to give 0.477 g of a colorless oil **23a** (yield: 90%). <sup>1</sup>H NMR (200 MHz, CDCl<sub>3</sub>) δ: 8.18 (d, 2H, J = 2.4 Hz), 7.79 (dd, 2H, J = 2.4 Hz, J = 8.6 Hz), 7.45 (d, 4H, J = 8.4 Hz), 7.23 (d, 4H, J = 8.6 Hz), 6.96 (s, 4H), 6.80 (d, 2H, J = 8.6 Hz), 4.49 (t, 4H, J = 4.8 Hz), 3.86 (t, 4H, J = 4.8 Hz), 3.64–3.79 (m, 29H), 3.49–3.58 (m, 4H), 3.27 (s, 6H), 1.47 (s, 18H).

2-(1,3-Di((E)-2-(2-(2-(2-(5-(4-(tert-butoxycarbonyl(methylamino)styryl)pyridin-2-yloxy)ethoxy)ethoxy)ethoxy)ethoxy)ethoxy)propan-2-yloxy)ethanol (**23b**). Compound **23b** was prepared from **22b** (0.128 g, 0.1 mmol) and PPTS (0.0025 g, 0.01 mmol) in 1 mL of EtOH, with the same procedure described for compound **23a**. Compound **23b**: 0.116 g (yield: 98%). <sup>1</sup>H NMR (200 MHz, CDCl<sub>3</sub>) δ: 8.19 (d, 2H, J = 2.2 Hz), 7.80 (dd, 2H, J = 2.6 Hz, J = 8.8 Hz), 7.45 (d, 4H, J = 8.6 Hz), 7.23 (d, 4H, J = 8.6 Hz), 6.97 (s, 4H), 6.80 (d, 2H, J = 8.6 Hz), 4.50 (t, 4H, J = 4.8 Hz), 3.87 (t, 4H, J = 4.8 Hz), 3.65–3.79 (m, 37H), 3.51–3.55 (m, 4H), 3.28 (s, 6H), 1.47 (s, 18H).

2-(1,3-Di((E)-2-(2-(2-(2-(5-(4-(tert-butoxycarbonyl(methylamino)styryl)pyridin-2-yloxy)ethoxy)ethoxy)ethoxy)ethoxy)ethoxy)propan-2-yloxy)ethanol (**23c**). Compound **23c** was prepared from **22c** (0.314 g, 0.23 mmol) and PPTS (0.00577 g, 0.023 mmol) in 2 mL of EtOH, with the same procedure described for compound **23a**. Compound **23c**: 0.235 g (yield: 80%). <sup>1</sup>H NMR (200 MHz, CDCl<sub>3</sub>) δ: 8.19 (d, 2H, J = 2.2 Hz), 7.80 (dd, 2H, J = 2.4 Hz, J = 8.8 Hz), 7.45 (d, 4H, J = 8.6 Hz), 7.23 (d, 4H, J = 8.6 Hz), 6.97 (s, 4H), 6.80 (d, 2H, J = 8.6 Hz), 4.50 (t, 4H, J = 4.8 Hz), 3.87 (t, 4H, J = 4.8 Hz), 3.64–3.71 (m, 45H), 3.51–3.55 (m, 4H), 3.28 (s, 6H), 1.47 (s, 18H).

2-(1,3-Di((E)-2-(2-(2-(2-(5-(4-(tert-butoxycarbonyl(methylamino)styryl)pyridin-2-yloxy)ethoxy)ethoxy)ethoxy)ethoxy)ethoxy)propan-2-yloxy)ethyl-4-methylbenzene Sulfonate (**24a**). To a solution of **23a** (0.395 g, 0.36 mmol) and triethylamine (0.180 g, 1.79 mmol) in 5 mL of DCM was added *p*-toluenesulfonyl chloride (0.135 g, 0.71 mmol) and DMAP (0.0044 g, 0.036 mmol) at 0 °C. The solution was allowed to warm to rt. After 1 h, the mixture was diluted with 30 mL of DCM, washed with H<sub>2</sub>O (10 mL × 2) as well as brine (10 mL). The organic layer was dried by Na<sub>2</sub>SO<sub>4</sub> and concentrated to give an oil that was purified by FC (DCM/MeOH = 95/5) to give 0.444 g of a yellowish solid **24a** (yield: 97%). <sup>1</sup>H NMR (200 MHz, CDCl<sub>3</sub>) δ: 8.18 (d, 2H, J = 2.0 Hz), 7.77–7.82 (m, 4H), 7.45 (d, 4H, J = 8.6 Hz), 7.33 (d, 2H, J = 8.0 Hz), 7.23 (d, 4H, J = 8.6 Hz),

6.97 (s, 4H), 6.79 (d, 2H,  $J = 8.6$  Hz), 4.50 (t, 4H,  $J = 4.8$  Hz), 4.15 (t, 2H,  $J = 4.8$  Hz), 3.80–3.89 (m, 6H), 3.55–3.74 (m, 25H), 3.44–3.51 (m, 4H), 3.28 (s, 6H), 2.44 (s, 3H), 1.47 (s, 18H).

**2-(1,3-Di((E)-2-(2-(2-(2-(5-(4-(tert-butoxycarbonyl(methyl)amino)styryl)pyridin-2-yloxy)ethoxy)ethoxy)ethoxy)ethoxy)ethoxy)propan-2-yloxy)ethyl-4-methylbenzene Sulfonate (24b).** Compound **24b** was prepared from **23b** (0.125 g, 0.11 mmol), triethylamine (0.0525 g, 0.5 mmol), *p*-toluenesulfonyl chloride (0.0400 g, 0.21 mmol), and DMAP (0.0012 g, 0.01 mmol) in 2 mL of DCM, with the same procedure described for compound **24a**. Compound **24b**: 0.134 g (yield: 96%).  $^1\text{H NMR}$  (200 MHz,  $\text{CDCl}_3$ )  $\delta$ : 8.19 (d, 2H,  $J = 2.0$  Hz), 7.77–7.82 (m, 4H), 7.45 (d, 4H,  $J = 8.6$  Hz), 7.34 (d, 2H,  $J = 8.4$  Hz), 7.23 (d, 4H,  $J = 8.8$  Hz), 6.97 (s, 4H), 6.79 (d, 2H,  $J = 8.6$  Hz), 4.50 (t, 4H,  $J = 4.8$  Hz), 4.14 (t, 2H,  $J = 4.8$  Hz), 3.80–3.89 (m, 6H), 3.60–3.74 (m, 33H), 3.46–3.51 (m, 4H), 3.28 (s, 6H), 2.44 (s, 3H), 1.47 (s, 18H).

**2-(1,3-Di((E)-2-(2-(2-(2-(5-(4-(tert-butoxycarbonyl(methyl)amino)styryl)pyridin-2-yloxy)ethoxy)ethoxy)ethoxy)ethoxy)ethoxy)propan-2-yloxy)ethyl-4-methylbenzenesulfonate (24c).** Compound **24c** was prepared from **23c** (0.230 g, 0.18 mmol), triethylamine (0.0909 g, 0.9 mmol), *p*-toluenesulfonyl chloride (0.0686 g, 0.36 mmol), and DMAP (0.0022 g, 0.018 mmol) in 3 mL of DCM, with the same procedure described for compound **24a**. Compound **24c**: 0.240 g (yield: 98%).  $^1\text{H NMR}$  (200 MHz,  $\text{CDCl}_3$ )  $\delta$ : 8.18 (d, 2H,  $J = 2.2$  Hz), 7.78–7.82 (m, 4H), 7.45 (d, 4H,  $J = 8.6$  Hz), 7.34 (d, 2H,  $J = 8.0$  Hz), 7.23 (d, 4H,  $J = 8.2$  Hz), 6.97 (s, 4H), 6.79 (d, 2H,  $J = 8.6$  Hz), 4.50 (t, 4H,  $J = 4.8$  Hz), 4.14 (t, 2H,  $J = 4.8$  Hz), 3.80–3.89 (m, 6H), 3.46–3.75 (m, 41H), 3.44–3.51 (m, 4H), 3.28 (s, 6H), 2.45 (s, 3H), 1.47 (s, 18H).

**2-(2-Fluoroethoxy)-1,3-di((E)-2-(2-(2-(2-(5-(4-(tert-butoxycarbonyl(methyl)amino)styryl)pyridin-2-yloxy)ethoxy)ethoxy)ethoxy)ethoxy)ethoxy)propane (25a).** A mixture of **24a** (0.126 g, 0.1 mmol) and tetrabutylammonium fluoride (TBAF, 0.25 mL, 1.0 M in THF) in 1.5 mL of THF was stirred at 70 °C overnight. The reaction mixture was evaporated in vacuo, and the residue was purified by FC (EtOAc/MeOH = 9/1) to give 0.054 g of a colorless oil **25a** (yield: 49%).  $^1\text{H NMR}$  (200 MHz,  $\text{CDCl}_3$ )  $\delta$ : 8.17 (d, 2H,  $J = 2.2$  Hz), 7.78 (dd, 2H,  $J = 2.2$  Hz,  $J = 8.6$  Hz), 7.43 (d, 4H,  $J = 8.6$  Hz), 7.22 (d, 4H,  $J = 8.6$  Hz), 6.96 (s, 4H), 6.78 (d, 2H,  $J = 8.6$  Hz), 4.64 (t, 1H,  $J = 4.2$  Hz), 4.48 (t, 4H,  $J = 4.8$  Hz), 4.40 (t, 1H,  $J = 4.2$  Hz), 3.94 (t, 1H,  $J = 4.3$  Hz), 3.85 (t, 4H,  $J = 4.8$  Hz), 3.79 (t, 1H,  $J = 4.3$  Hz), 3.62–3.73 (m, 25H), 3.54–3.58 (m, 4H), 3.26 (s, 6H), 1.46 (s, 18H).

**2-(2-Fluoroethoxy)-1,3-di((E)-2-(2-(2-(2-(5-(4-(tert-butoxycarbonyl(methyl)amino)styryl)pyridin-2-yloxy)ethoxy)ethoxy)ethoxy)ethoxy)ethoxy)propane (25b).** Compound **25b** was prepared from **24b** (0.100 g, 0.074 mmol) and TBAF (0.15 mL, 1.0 M in THF) in 1 mL THF, with the same procedure described for compound **25a**. Compound **25b**: 0.0726 g (yield: 82%).  $^1\text{H NMR}$  (200 MHz,  $\text{CDCl}_3$ )  $\delta$ : 8.18 (d, 2H,  $J = 2.2$  Hz), 7.79 (dd, 2H,  $J = 2.4$  Hz,  $J = 8.6$  Hz), 7.45 (d, 4H,  $J = 8.6$  Hz), 7.23 (d, 4H,  $J = 8.6$  Hz), 6.97 (s, 4H), 6.79 (d, 2H,  $J = 8.6$  Hz), 4.65 (t, 1H,  $J = 4.2$  Hz), 4.50 (t, 4H,  $J = 4.8$  Hz), 4.41 (t, 1H,  $J = 4.2$  Hz), 3.95 (t, 1H,  $J = 4.3$  Hz), 3.78–3.89 (m, 5H), 3.53–3.77 (m, 37H), 3.28 (s, 6H), 1.47 (s, 18H).

**2-(2-Fluoroethoxy)-1,3-di((E)-2-(2-(2-(2-(5-(4-(tert-butoxycarbonyl(methyl)amino)styryl)pyridin-2-yloxy)ethoxy)ethoxy)ethoxy)ethoxy)ethoxy)propane (25c).** Compound **25c** was prepared from **24c** (0.171 g, 0.12 mmol) and TBAF (0.24 mL, 1.0 M in THF) in 2 mL THF, with the same procedure described for compound **25a**. Compound **25c**: 0.123 g (yield: 80%).  $^1\text{H NMR}$  (200 MHz,  $\text{CDCl}_3$ )  $\delta$ : 8.19 (d, 2H,  $J = 2.2$  Hz), 7.80 (dd, 2H,  $J = 2.4$  Hz,  $J = 8.6$  Hz), 7.45 (d, 4H,  $J = 8.6$  Hz), 7.23 (d, 4H,  $J = 8.6$  Hz), 6.98 (s, 4H), 6.80 (d, 2H,  $J = 8.6$  Hz), 4.65 (t, 1H,  $J = 4.2$  Hz), 4.50 (t, 4H,  $J = 4.8$  Hz), 4.42 (t, 1H,  $J = 4.2$  Hz), 3.96 (t, 1H,  $J = 4.3$  Hz), 3.78–3.89 (m, 5H), 3.53–3.77 (m, 45H), 3.28 (s, 6H), 1.47 (s, 18H).

**Ethyl 2-(2-(2-(Hydroxyethoxy)ethoxy)ethoxy)acetate (26).** To a solution of tetraethylene glycol (3.02 g, 20 mmol) and boron trifluoride–diethyl ether (0.1 mL) in 40 mL of DCM was slowly added ethyl diazoacetate (1.14 g, 10 mmol) in 10 mL of DCM at 0 °C. The reaction mixture was stirred at rt for 2 h and then washed with  $\text{H}_2\text{O}$  (10 mL  $\times$  2) as well as brine (10 mL). The organic layer was dried by  $\text{Na}_2\text{SO}_4$  and concentrated to give 1.19 g of a clear oil **26**

(yield: 50%).  $^1\text{H NMR}$  (200 MHz,  $\text{CDCl}_3$ )  $\delta$ : 4.16–4.28 (m, 4H), 3.60–3.76 (m, 12H), 2.43 (t, 1H,  $J = 6.2$  Hz), 1.30 (t, 3H,  $J = 7.2$  Hz).

**Ethyl 2-(2-(2-(2-Bromoethoxy)ethoxy)ethoxy)acetate (27).** To a solution of triphenylphosphine (2.16 g, 8.25 mmol) and *N*-bromosuccinimide (1.47 g, 8.25 mmol) in 30 mL of DCM was slowly added **26** (1.30 g, 5.5 mmol) in 20 mL of DCM at 0 °C. The reaction mixture was stirred at 0 °C for 2 h and then washed with  $\text{H}_2\text{O}$  (10 mL  $\times$  2) and brine (10 mL). The organic layer was dried by  $\text{Na}_2\text{SO}_4$  and concentrated to give 1.39 g of yellow oil **27** (yield: 85%).  $^1\text{H NMR}$  (200 MHz,  $\text{CDCl}_3$ )  $\delta$ : 4.16–4.28 (m, 4H), 3.68–3.86 (m, 10H), 3.48 (t, 2H,  $J = 6.4$  Hz), 1.29 (t, 3H,  $J = 7.2$  Hz).

**2-(2-(2-(2-Bromoethoxy)ethoxy)ethoxy)acetic Acid (28).** A solution of **27** (1.39 g, 4.6 mmol) in 15 mL of sodium hydroxide (NaOH, 1 M)/THF (v/v, 1/1) was stirred at rt for 2 h. Hydrochloric acid (HCl, 0.9 mL) was then added to the mixture. The solvent was removed in vacuo, and the residue was taken up in DCM. The mixture was filtered, and the filtrate was concentrated to give 0.810 g of clear oil **28** (yield: 65%).  $^1\text{H NMR}$  (200 MHz,  $\text{CDCl}_3$ )  $\delta$ : 4.17 (s, 2H), 3.75–3.88 (m, 10H), 3.52 (t, 2H,  $J = 6.4$  Hz).

**tert-Butyl 14-Bromo-3-(2-tert-butoxy-2-oxoethyl)-4-oxo-6,9,12-trioxo-3-azatetradecan-1-oate (29).** To a solution of **28** (0.810 g, 2.9 mmol) in 15 mL of DMF was added di-*tert*-butyl iminodiacetate (0.711 g, 2.9 mmol), 1-hydroxybenzotriazole hydrate (0.882 g, 5.22 mmol), *N*-(3-dimethylaminopropyl)-*N'*-ethylcarbodiimide hydrochloride (1.0 g, 5.22 mmol), and *N,N*-diisopropylethylamine (0.674 g, 5.22 mmol). After stirring at rt overnight, the mixture was poured into 100 mL of EtOAc and washed with  $\text{H}_2\text{O}$  (30 mL  $\times$  2) and brine (30 mL). The organic layer was dried by  $\text{Na}_2\text{SO}_4$  and filtered. The filtrate was concentrated, and the residue was purified by FC (EtOAc/hexane = 1/1) to give 0.931 g of clear oil **29** (yield: 64%).  $^1\text{H NMR}$  (200 MHz,  $\text{CDCl}_3$ )  $\delta$ : 4.24 (s, 2H), 4.14 (s, 2H), 4.05 (s, 2H), 3.64–3.86 (m, 10H), 3.48 (t, 2H,  $J = 6.4$  Hz), 1.49 (s, 9H), 1.47 (s, 9H).

**14-Bromo-3-(carboxymethyl)-4-oxo-6,9,12-trioxo-3-azatetradecan-1-oic Acid (30).** A solution of **29** (0.157 g, 0.3 mmol) in 3 mL of TFA/DCM (v/v, 1/1) was stirred at rt for 2 h. Removal of solvent gave clear oil. After several times of coevaporation with methanol, 0.112 g of **30** (yield: 97%) was given as a clear oil.  $^1\text{H NMR}$  (200 MHz,  $\text{CDCl}_3$ )  $\delta$ : 4.49 (s, 2H), 4.34 (s, 2H), 4.28 (s, 2H), 3.74–3.92 (m, 10H), 3.49 (t, 2H,  $J = 6.0$  Hz).

**(E)-tert-Butyl 4-(2-(6-(2-(2-(2-(2-Azidoethoxy)ethoxy)ethoxy)ethoxy)pyridin-3-yl)vinyl)phenyl(methyl)carbamate (31).** Sodium azide (0.566 g, 8.7 mmol) was added to a solution of **15a** (1.91 g, 2.9 mmol) in 20 mL of DMF. After stirring at 60 °C for 3 h, the mixture was then poured into 100 mL of EtOAc and washed with  $\text{H}_2\text{O}$  (30 mL  $\times$  2) as well as brine (30 mL). The organic layer was dried by  $\text{Na}_2\text{SO}_4$  and filtered. The filtrate was concentrated, and the residue was purified by FC (EtOAc/hexane = 1/1) to give 1.33 g of white solid **31** (yield: 87%).  $^1\text{H NMR}$  (200 MHz,  $\text{CDCl}_3$ )  $\delta$ : 8.20 (d, 1H,  $J = 2.6$  Hz), 7.80 (dd, 1H,  $J = 2.2$  Hz,  $J = 8.6$  Hz), 7.45 (d, 2H,  $J = 8.4$  Hz), 7.23 (d, 2H,  $J = 8.6$  Hz), 6.98 (s, 2H), 6.81 (d, 1H,  $J = 8.4$  Hz), 4.51 (t, 2H,  $J = 4.8$  Hz), 3.88 (t, 2H,  $J = 4.8$  Hz), 3.66–3.72 (m, 10H), 3.39 (t, 2H,  $J = 4.8$  Hz), 3.28 (s, 3H), 1.47 (s, 9H).

**(E)-tert-Butyl 4-(2-(6-(2-(2-(2-(2-Aminoethoxy)ethoxy)ethoxy)ethoxy)pyridin-3-yl)vinyl)phenyl(methyl)carbamate (32).** Triphenylphosphine (0.472 g, 1.8 mmol) was added to a solution of **31** (0.379 g, 0.72 mmol) in 12.6 mL of THF. After stirring at rt for 2 h, 1.4 mL of  $\text{H}_2\text{O}$  was added and the mixture was heated at 60 °C overnight. The reaction mixture was evaporated in vacuo, and the residue was purified by FC (DCM/MeOH/ $\text{NH}_4\text{OH} = 90/9/1$ ) to give 0.360 g of white solid **32** (yield: 100%).  $^1\text{H NMR}$  (200 MHz,  $\text{CDCl}_3$ )  $\delta$ : 8.19 (d, 1H,  $J = 2.4$  Hz), 7.81 (dd, 1H,  $J = 2.4$  Hz,  $J = 8.6$  Hz), 7.45 (d, 2H,  $J = 8.4$  Hz), 7.23 (d, 2H,  $J = 8.6$  Hz), 6.98 (s, 2H), 6.81 (d, 1H,  $J = 8.8$  Hz), 4.50 (t, 2H,  $J = 4.8$  Hz), 3.88 (t, 2H,  $J = 4.8$  Hz), 3.67–3.72 (m, 8H), 3.56 (t, 2H,  $J = 5.2$  Hz), 3.28 (s, 3H), 2.890 (t, 2H,  $J = 5.2$  Hz), 1.47 (s, 9H).

**2-(2-(2-(2-Bromoethoxy)ethoxy)ethoxy)-*N,N*-bis(2-(((E)-2-(2-(2-(2-(5-(4-(tert-butoxycarbonyl(methyl)amino)styryl)pyridin-2-yloxy)ethoxy)ethoxy)ethoxy)ethoxy)amino)-2-oxoethyl)acetamide (33).** To a solution of **30** (0.116 g, 0.3 mmol) in 6 mL of DCM was added *N,N'*-dicyclohexylcarbodiimide (0.247 g, 1.2 mmol), **32** (0.301 g,

0.6 mmol), and 4-(dimethylamino)pyridine (0.0073 g, 0.06 mmol). The mixture was stirred at rt for 3 h and filtered with Celite. The filtrate was concentrated, and the residue was purified by FC (DCM/MeOH/NH<sub>4</sub>OH = 95/5/0.5) to give 0.161 g of clear oil **33** (yield: 40%). <sup>1</sup>H NMR (200 MHz, CDCl<sub>3</sub>) δ: 8.19 (d, 2H, J = 2.2 Hz), 7.80 (dd, 2H, J = 2.2 Hz, J = 8.6 Hz), 7.45 (d, 4H, J = 8.4 Hz), 7.23 (d, 4H, J = 8.4 Hz), 6.97 (s, 4H), 6.79 (dd, 2H, J = 3.4 Hz, J = 8.8 Hz), 4.50 (t, 4H, J = 4.8 Hz), 4.18 (s, 2H), 4.12 (s, 2H), 3.97 (s, 2H), 3.78–3.86 (m, 6H), 3.58–3.70 (m, 28H), 3.44–3.50 (m, 6H), 3.28 (s, 6H), 1.47 (s, 18H).

*N,N*-Bis(2-((*E*)-2-(2-(2-(2-(5-(4-(*tert*-butoxycarbonyl(methyl)amino)styryl)pyridin-2-yloxy)ethoxy)ethoxy)ethoxy)ethyl)-1*H*-1,2,3-triazol-4-yl)methoxy)-2-((*E*)-(1-(2-(2-(2-(2-(5-(4-(*tert*-butoxycarbonyl(methyl)amino)styryl)pyridin-2-yloxy)ethoxy)ethoxy)ethoxy)ethyl)-1*H*-1,2,3-triazol-4-yl)methoxy)methyl)propane (**34**). A mixture of **33** (0.100 g, 0.074 mmol) and TBAF (0.15 mL, 1.0 M in THF) in 1 mL of THF was stirred at 70 °C overnight. The reaction mixture was evaporated in vacuo, and the residue was purified by FC (DCM/MeOH/NH<sub>4</sub>OH = 95/5/0.5) to give 0.045 g clear oil **34** (yield: 47%). <sup>1</sup>H NMR (200 MHz, CDCl<sub>3</sub>) δ: 8.17 (d, 2H, J = 2.2 Hz), 7.79 (dd, 2H, J = 2.4 Hz, J = 8.6 Hz), 7.44 (d, 4H, J = 8.6 Hz), 7.22 (d, 4H, J = 8.4 Hz), 6.96 (s, 4H), 6.78 (dd, 2H, J = 2.2 Hz, J = 8.6 Hz), 4.67 (t, 1H, J = 4.1 Hz), 4.41–4.51 (m, 5H), 4.17 (s, 2H), 4.12 (s, 2H), 3.97 (s, 2H), 3.50–3.88 (m, 34H), 3.43–3.48 (m, 4H), 3.27 (s, 6H), 1.46 (s, 18H).

3-(*Prop*-2-ynyloxy)-2,2-bis((*prop*-2-ynyloxy)methyl)propan-1-ol (**35**). An aqueous solution of NaOH (40 wt %, 10 mL) was added to a solution of pentaerythritol (2.00 g, 14.7 mmol) in 15 mL of dimethylsulfoxide (DMSO). The solution was stirred at rt for 30 min. Propargyl bromide (97%, 9.8 mL, 110 mmol) was then added, and the solution was kept at rt for an additional 10 h. The reaction mixture was then poured into 150 mL of EtOAc and washed with H<sub>2</sub>O (50 mL × 2) as well as brine (50 mL). The organic layer was dried by Na<sub>2</sub>SO<sub>4</sub> and filtered. The filtrate was concentrated, and the residue was purified by FC (EtOAc/hexane = 1/4) to give 2.29 g of yellowish oil **35** (yield: 62%). <sup>1</sup>H NMR (200 MHz, CDCl<sub>3</sub>) δ: 4.13 (d, 6H, J = 2.4 Hz), 3.69 (d, 2H, J = 6.4 Hz), 3.56 (s, 6H), 2.43 (t, 3H, J = 2.4 Hz).

11,11-Bis((*prop*-2-ynyloxy)methyl)-3,6,9,13-tetraoxahexadec-15-ynyl 4-Methylbenzenesulfonate (**36**). NaH (60% in mineral oil, 0.120 g, 3.0 mmol) was placed in a two-neck flask and washed with hexane. Six mL of DMF was added to form a suspension. A solution of **35** (0.500 g, 2.0 mmol) in 4 mL of DMF was added dropwise at 0 °C. After stirring at rt for 30 min, the mixture was cooled to 0 °C, and a solution of triethylene glycol di(*p*-toluenesulfonate) (1.38 g, 3.0 mmol) in 3 mL of DMF was added dropwise. After stirred at rt overnight, the mixture was poured into 50 mL cold satd NH<sub>4</sub>Cl and extracted with DCM (30 mL × 2). The organic layer was washed with H<sub>2</sub>O (20 mL) and brine (20 mL), dried over Na<sub>2</sub>SO<sub>4</sub>, concentrated, and purified by FC (EtOAc/hexane = 3/7) to give 0.501 g colorless oil **36** (yield: 47%). <sup>1</sup>H NMR (200 MHz, CDCl<sub>3</sub>) δ: 7.81 (d, 2H, J = 8.4 Hz), 7.35 (d, 2H, J = 8.4 Hz), 4.11–4.20 (m, 8H), 3.71 (t, 2H, J = 4.8 Hz), 3.58–3.60 (m, 8H), 3.52 (s, 6H), 3.45 (s, 2H), 2.46 (s, 3H), 2.41 (t, 3H, J = 2.4 Hz).

1-Fluoro-11,11-bis((*prop*-2-ynyloxy)methyl)-3,6,9,13-tetraoxahexadec-15-yne (**37**). A mixture of **36** (0.200 g, 0.37 mmol) and TBAF (1.12 mL, 1.0 M in THF) in 4 mL of THF was stirred at 70 °C overnight. The reaction mixture was evaporated in vacuo, and the residue was purified by FC (EtOAc/hexane = 3/7) to give 0.122 g of clear oil **37** (yield: 86%). <sup>1</sup>H NMR (200 MHz, CDCl<sub>3</sub>) δ: 4.69 (t, 1H, J = 4.2 Hz), 4.46 (t, 1H, J = 4.2 Hz), 4.13 (d, 6H, J = 2.4 Hz), 3.84 (t, 1H, J = 4.2 Hz), 3.67–3.71 (m, 5H), 3.59–3.64 (m, 4H), 3.54 (s, 6H), 3.47 (s, 2H), 2.41 (t, 3H, J = 2.4 Hz).

2-(2-(3-(*E*)-(1-(2-(2-(2-(5-(4-(*tert*-butoxycarbonyl(methyl)amino)styryl)pyridin-2-yloxy)ethoxy)ethoxy)ethyl)-1*H*-1,2,3-triazol-4-yl)methoxy)-2,2-bis((*E*)-(1-(2-(2-(2-(2-(5-(4-(*tert*-butoxycarbonyl(methyl)amino)styryl)pyridin-2-yloxy)ethoxy)ethoxy)ethyl)-1*H*-1,2,3-triazol-4-yl)methoxy)methyl)propoxy)ethoxy)ethyl 4-Methylbenzenesulfonate (**38**). A solution of **36** (0.0313 g, 0.058 mmol), **31** (0.0923 g, 0.175 mmol), sodium ascorbate (0.0174 g, 0.088 mmol), and copper sulfate (CuSO<sub>4</sub>, 0.0028 g, 0.0175 mmol) in 2 mL of *t*-BuOH/H<sub>2</sub>O (v/v, 1/1) was stirred at rt for 4 h. The reaction mixture was then poured into 10 mL of EtOAc and washed with H<sub>2</sub>O (3 mL × 2) and brine (3 mL).

The organic layer was dried by Na<sub>2</sub>SO<sub>4</sub> and filtered. The filtrate was concentrated, and the residue was purified by FC (EtOAc/MeOH = 9/1) to give 0.110 g clear oil **38** (yield: 90%). <sup>1</sup>H NMR (200 MHz, CDCl<sub>3</sub>) δ: 8.17 (d, 3H, J = 2.2 Hz), 7.76–7.82 (m, 5H), 7.71 (s, 3H), 7.45 (d, 6H, J = 8.6 Hz), 7.33 (d, 2H, J = 8.2 Hz), 7.23 (d, 6H, J = 8.6 Hz), 6.97 (s, 6H), 6.77 (d, 3H, J = 8.6 Hz), 4.46–4.59 (m, 18H), 4.11–4.16 (m, 2H), 3.83–3.90 (m, 12H), 3.61–3.71 (m, 26H), 3.38–3.56 (m, 16H), 3.28 (s, 9H), 2.43 (s, 3H), 1.47 (s, 27H).

1,3-Di(*E*)-(1-(2-(2-(2-(2-(5-(4-(*tert*-butoxycarbonyl(methyl)amino)styryl)pyridin-2-yloxy)ethoxy)ethoxy)ethyl)-1*H*-1,2,3-triazol-4-yl)methoxy)-2-((*E*)-(1-(2-(2-(2-(2-(5-(4-(*tert*-butoxycarbonyl(methyl)amino)styryl)pyridin-2-yloxy)ethoxy)ethoxy)ethyl)-1*H*-1,2,3-triazol-4-yl)methoxy)methyl)-2-((2-(2-(2-fluoroethoxy)ethoxy)ethoxy)methyl)propane (**39**). Compound **39** was prepared from **37** (0.0486 g, 0.126 mmol), **31** (0.201 g, 0.38 mmol), sodium ascorbate (0.0376 g, 0.19 mmol), and CuSO<sub>4</sub> (0.0061 g, 0.038 mmol) in 4 mL of *t*-BuOH/H<sub>2</sub>O (v/v, 1/1), with the same procedure described for compound **38**. Compound **39**: 0.208 g (yield: 84%). <sup>1</sup>H NMR (200 MHz, CDCl<sub>3</sub>): 8.17 (d, 3H, J = 2.4 Hz), 7.79 (dd, 3H, J = 2.4 Hz, J = 8.6 Hz), 7.71 (s, 3H), 7.45 (d, 6H, J = 8.6 Hz), 7.23 (d, 6H, J = 8.6 Hz), 6.97 (s, 6H), 6.77 (dd, 3H, J = 8.6 Hz), 4.65 (t, 1H, J = 4.2 Hz), 4.39–4.60 (m, 19H), 3.77–3.90 (m, 13H), 3.43–3.73 (m, 41H), 3.28 (s, 9H), 1.47 (s, 27H).

**2. Radiosynthesis of [<sup>18</sup>F]8a–c.** Preparation of [<sup>18</sup>F]8a–c was achieved by using a modified method reported previously (see Scheme S).<sup>27</sup> Briefly, the <sup>18</sup>F-fluoride ions were trapped on an activated QMA anion exchange cartridge and eluted with 1 mL of Kryptofix222/K<sub>2</sub>CO<sub>3</sub> acetonitrile/water solution (22 mg Kryptofix222/1.8 mg K<sub>2</sub>CO<sub>3</sub>/0.84 mL ACN/0.16 mL water). The solution was azeotropically dried twice with acetonitrile at 110 °C under a stream of argon. Approximately 1 mg of *O*-tosylated precursor (**24a–c**) was dissolved in 1 mL of DMSO and added to the anhydrous Kryptofix/K<sub>2</sub>CO<sub>3</sub>/[<sup>18</sup>F]fluoride. The reaction was heated for 10 min at 110 °C and allowed to cool at room temperature for 5 min. One mL of a 10% (~4 N) HCl solution was added and heated at 80 °C for 7 min. The reaction was cooled in an ice bath, neutralized with a NaOH solution, and diluted with water to about 8 mL total volume. The mixture was pushed through an activated C4 mini column (Vydac Bioselect 214SPE3000 reversed-phase C4), washed twice with 3 mL of water and [<sup>18</sup>F]8a–c was eluted with 1 mL of ethanol (decay corrected radiochemical yields were 29%, 29%, and 30%, respectively; radiochemical purity was >98%). To ensure an accurate detection of free fluoride, other impurities and the desired products, [<sup>18</sup>F]8a–c, two HPLC systems were employed: (a) Gemini C18 150 mm × 4.6 mm, acetonitrile/10 mM ammonium formate buffer 8/2 and flow rate of 1 mL/min and (b) Gemini C18 250 mm × 4.6 mm with a solvent gradient at a flow rate of 1 mL/min according to the following: 0–2 min 100% 10 mM ammonium formate buffer; 2–5 min ammonium formate buffer 100% to 30%, ACN 0% to 70%; 5–10 min ammonium formate buffer 30% to 0%, ACN 70% to 100%, 10–15 min ammonium formate buffer 0% to 100%, 15–18 min 100% ammonium formate buffer.

**3. In Vitro Autoradiography of AD Brain Sections.** Frozen brains from confirmed CAA, AD, and control subjects were cut into 20 μm sections. The sections were incubated with the <sup>18</sup>F labeled tracer in 40% ethanol for 1 h. The sections were then dipped in saturated Li<sub>2</sub>CO<sub>3</sub> in 40% ethanol (2 min wash, twice) and washed with 40% ethanol (2 min wash, once), followed by rinsing with water for 30 s. After drying, the sections were exposed to Kodak Biomax MR film for 12–18 h. After the film was developed, the images were digitized.

**4. Thioflavin S Staining.** Brain sections were immersed in 10% neutral buffered formalin for 1 h and then treated with 0.05% KMnO<sub>4</sub> and bleached in 0.2% K<sub>2</sub>S<sub>2</sub>O<sub>5</sub>/0.2% oxalic acid in order to quench autofluorescence. Quenched tissue sections were stained with 0.025% thioflavin S in 40% ethanol for 3–5 min. The sections were differentiated in 50% ethanol and viewed using a Nikon E800 fluorescence microscope with a CCD digital camera.

**5. In Vivo Biodistribution Study in ICR Mice.** To test [<sup>18</sup>F]8a–c as PET imaging agents for cerebral amyloid angiopathy, we first tested the biodistribution of these tracers in normal ICR mice

(20–25 g). A group of 5–6 mice were used for each time point of the biodistribution studies. After the mice were put under anesthesia with isoflurane (2–3%), 0.15 mL of saline solution containing 925 KBq (25  $\mu$ Ci) of the tracer was injected via the lateral tail vein. The mice were sacrificed at 2 and 30 min postinjection by cardiac excision while under isoflurane anesthesia. The organs of interest were removed, weighed, and the radioactivity was counted with a  $\gamma$  counter (Packard Cobra). The percent dose per gram was calculated by a comparison of the tissue activity counts to counts of 1% of the initial dose. The initial dose was measured by aliquots of the injected material diluted 100 times and measured at the same time (0.5 min/sample, 80% efficiency).

## ■ ASSOCIATED CONTENT

### ● Supporting Information

Method for in vitro binding assay and HPLC profiles of final tested compounds. This material is available free of charge via the Internet at <http://pubs.acs.org>.

## ■ AUTHOR INFORMATION

### Corresponding Author

\*Phone: (215) 662-3096. Fax: (215) 349-5035. E-mail: [kunghf@gmail.com](mailto:kunghf@gmail.com). Address: Hank F. Kung, Ph.D., 3700 Market Street, Suite 305, Department of Radiology, University of Pennsylvania School of Medicine, Philadelphia, PA 19104.

## ■ ACKNOWLEDGMENTS

This work was supported by grants from the National Institutes of Health (RO1-AG-022559 (H.F.K.) and R43AG032206 (D.S.)) and Avid Radiopharmaceuticals Inc. We thank Dr. Carita Huang for editing and reviewing this manuscript. The authors thank Dr. Nick Bryan for his encouragement and helpful discussion.

## ■ ABBREVIATIONS USED

AD, Alzheimer's disease; A $\beta$ ,  $\beta$ -amyloid; CAA, cerebral amyloid angiopathy; APP,  $\beta$ -amyloid precursor protein; PET, positron emission tomography; PIB, Pittsburgh compound B; SB-13, 4-*N*-methylamino-4'-hydroxystilbene; IMPY, 6-[iodo-2-(4'-*N,N*-dimethylamino)-phenylimidazo[1,2-*a*]pyridine; [<sup>18</sup>F]AV-1, BAY-94-9172, [<sup>18</sup>F]florbetaben f 18; [<sup>18</sup>F]AV-45, [<sup>18</sup>F]-florbetapir f 18; [<sup>18</sup>F]FPIB, GE067, [<sup>18</sup>F]flutemetamol f 18; [<sup>18</sup>F]AZD4694, 2-(2-([<sup>18</sup>F]fluoro)-6-methylaminopyridin-3-yl)benzofuran-5-ol

## ■ REFERENCES

- (1) Soontornniyomkij, V.; Choi, C.; Pomakian, J.; Vinters, H. V. High-definition characterization of cerebral beta-amyloid angiopathy in Alzheimer's disease. *Hum. Pathol.* **2010**, *41*, 1601–1608.
- (2) Fisher, M.; French, S.; Ji, P.; Kim, R. C. Cerebral microbleeds in the elderly: a pathological analysis. *Stroke* **2010**, *41*, 2782–2785.
- (3) Cordonnier, C. Brain microbleeds: more evidence, but still a clinical dilemma. *Curr. Opin. Neurol.* **2011**, *24*, 69–74.
- (4) Altmann-Schneider, I.; Trompet, S.; de Craen, A. J.; van Es, A. C.; Jukema, J. W.; Stott, D. J.; Sattar, N.; Westendorp, R. G.; van Buchem, M. A.; van der Grond, J. Cerebral microbleeds are predictive of mortality in the elderly. *Stroke* **2011**, *42*, 638–644.
- (5) Poels, M. M.; Ikram, M. A.; van der Lugt, A.; Hofman, A.; Krestin, G. P.; Breteler, M. M.; Vernooij, M. W. Incidence of cerebral microbleeds in the general population: the Rotterdam scan study. *Stroke* **2011**, *42*, 656–661.
- (6) Dierksen, G. A.; Skehan, M. E.; Khan, M. A.; Jeng, J.; Nandigam, R. N.; Becker, J. A.; Kumar, A.; Neal, K. L.; Betensky, R. A.; Frosch, M. P.; Rosand, J.; Johnson, K. A.; Viswanathan, A.; Salat, D. H.; Greenberg, S. M. Spatial relation between microbleeds and amyloid deposits in amyloid angiopathy. *Ann. Neurol.* **2010**, *68*, 545–548.
- (7) Weller, R. O.; Boche, D.; Nicoll, J. A. Microvasculature changes and cerebral amyloid angiopathy in Alzheimer's disease and their potential impact on therapy. *Acta Neuropathol.* **2009**, *118*, 87–102.
- (8) Weller, R.; Preston, S.; Subash, M.; Carare, R. Cerebral amyloid angiopathy in the aetiology and immunotherapy of Alzheimer disease. *Alzheimers Res. Ther.* **2009**, *1*, 6.
- (9) Attems, J.; Jellinger, K. A.; Lintner, F. Alzheimer's disease pathology influences severity and topographical distribution of cerebral amyloid angiopathy. *Acta Neuropathol.* **2005**, *110*, 222–231.
- (10) Attems, J. Sporadic cerebral amyloid angiopathy: pathology, clinical implications, and possible pathomechanisms. *Acta Neuropathol.* **2005**, *110*, 345–359.
- (11) Attems, J.; Lintner, F.; Jellinger, K. A. Amyloid beta peptide 1–42 highly correlates with capillary cerebral amyloid angiopathy and Alzheimer disease pathology. *Acta Neuropathol.* **2004**, *107*, 283–291.
- (12) Jellinger, K. A.; Attems, J. Prevalence and pathogenic role of cerebrovascular lesions in Alzheimer disease. *J. Neurol. Sci.* **2005**, *229–230*, 37–41.
- (13) Jack, C. R. Jr.; Wiste, H. J.; Vemuri, P.; Weigand, S. D.; Senjem, M. L.; Zeng, G.; Bernstein, M. A.; Gunter, J. L.; Pankratz, V. S.; Aisen, P. S.; Weiner, M. W.; Petersen, R. C.; Shaw, L. M.; Trojanowski, J. Q.; Knopman, D. S. Brain beta-amyloid measures and magnetic resonance imaging atrophy both predict time-to-progression from mild cognitive impairment to Alzheimer's disease. *Brain* **2010**, *133*, 3336–3348.
- (14) Rinne, J.; Brooks, D.; Rossor, M.; Fox, N.; Bullock, R.; Klunk, W.; Mathis, C.; Blennow, K.; Barakos, J.; Okello, A.; Rodriguez Martinez de Liano, S.; Liu, E.; Koller, M.; Gregg, K.; Schenk, D.; Black, R.; Grundman, M. 11C-PiB PET assessment of change in fibrillar amyloid-beta load in patients with Alzheimer's disease treated with bapineuzumab: a phase 2, double-blind, placebo-controlled, ascending-dose study. *Lancet Neurol.* **2010**, *9*, 363–372.
- (15) Weiner, M.; Aisen, P.; Jack, C. Jr.; Jagust, W.; Trojanowski, J.; Shaw, L.; Saykin, A.; Morris, J.; Cairns, N.; Beckett, L.; Toga, A.; Green, R.; Walter, S.; Soares, H.; Snyder, P.; Siemers, E.; Potter, W.; Cole, P.; Schmidt, M. The Alzheimer's disease neuroimaging initiative: progress report and future plans. *Alzheimer's Dementia* **2010**, *6*, 202–211.e7.
- (16) Ikonovic, M. D.; Klunk, W. E.; Abrahamson, E. E.; Mathis, C. A.; Price, J. C.; Tsopelas, N. D.; Lopresti, B. J.; Ziolkowski, S.; Bi, W.; Paljug, W. R.; Debnath, M. L.; Hope, C. E.; Isanski, B. A.; Hamilton, R. L.; Dekosky, S. T. Post-mortem correlates of in vivo PiB-PET amyloid imaging in a typical case of Alzheimer's disease. *Brain* **2008**, *131*, 1630–1645.
- (17) Mok, V.; Leung, E.; Chu, W.; Chen, S.; Wong, A.; Xiong, Y.; Lam, W.; Ho, C.; Wong, K. Pittsburgh compound B binding in poststroke dementia. *J. Neurol. Sci.* **2010**, *290*, 135–137.
- (18) Ly, J.; Donnan, G.; Villemagne, V.; Zavala, J.; Ma, H.; O'Keefe, G.; Gong, S.; Gunawan, R.; Saunderson, T.; Ackerman, U.; Tchondanguy, H.; Churilov, L.; Phan, T.; Rowe, C. 11C-PIB binding is increased in patients with cerebral amyloid angiopathy-related hemorrhage. *Neurology* **2010**, *74*, 487–493.
- (19) Johnson, K. A.; Gregas, M.; Becker, J. A.; Kinnecom, C.; Salat, D. H.; Moran, E. K.; Smith, E. E.; Rosand, J.; Rentz, D. M.; Klunk, W. E.; Mathis, C. A.; Price, J. C.; Dekosky, S. T.; Fischman, A. J.; Greenberg, S. M. Imaging of amyloid burden and distribution in cerebral amyloid angiopathy. *Ann. Neurol.* **2007**, *62*, 229–234.
- (20) Wong, D.; Rosenberg, P.; Zhou, Y.; Kumar, A.; Raymond, V.; Ravert, H.; Dannals, R.; Nandi, A.; Brasic, J.; Ye, W.; Hilton, J.; Lyketsos, C.; Kung, H.; Joshi, A.; Skovronsky, D.; Pontecorvo, M. In Vivo Imaging of Amyloid Deposition in Alzheimer Disease Using the Radioligand 18F-AV-45 (Flobetapir F 18). *J. Nucl. Med.* **2010**, *51*, 913–920.
- (21) Kung, H.; Choi, S.; Qu, W.; Zhang, W.; Skovronsky, D. (18)F Stilbenes and Styrylpyridines for PET Imaging of Abeta Plaques in Alzheimer's Disease: A Miniperspective. *J. Med. Chem.* **2009**, *53*, 933–941.
- (22) Choi, S.; Golding, G.; Zhuang, Z.; Zhang, W.; Lim, N.; Hefti, F.; Benedum, T.; Kilbourn, M.; Skovronsky, D.; Kung, H. Preclinical

properties of 18F-AV-45: a PET agent for A $\beta$  plaques in the brain. *J. Nucl. Med.* **2009**, *50*, 1887–1894.

(23) Zhang, W.; Kung, M.; Oya, S.; Hou, C.; Kung, H. (18)F-labeled styrylpyridines as PET agents for amyloid plaque imaging. *Nucl. Med. Biol.* **2007**, *34*, 89–97.

(24) Clark, C. M.; Schneider, J. A.; Bedell, B. J.; Beach, T. G.; Bilker, W. B.; Mintun, M. A.; Pontecorvo, M. J.; Hefti, F.; Carpenter, A. P.; Flitter, M. L.; Krautkramer, M. J.; Kung, H. F.; Coleman, R. E.; Doraiswamy, P. M.; Fleisher, A. S.; Sabbagh, M. N.; Sadowsky, C. H.; Reiman, E. P.; Zehntner, S. P.; Skovronsky, D. M. Use of florbetapir-PET for imaging beta-amyloid pathology. *JAMA, J. Am. Med. Assoc.* **2011**, *305*, 275–283.

(25) O'Keefe, G.; Saunderson, T.; Ng, S.; Ackerman, U.; Tochon-Danguy, H.; Chan, J.; Gong, S.; Dyrks, T.; Lindemann, S.; Holl, G.; Dinkelborg, L.; Villemagne, V.; Rowe, C. Radiation Dosimetry of {beta}-Amyloid Tracers 11C-PiB and 18F-BAY94–9172. *J. Nucl. Med.* **2009**, *50*, 309–315.

(26) Rowe, C.; Ackerman, U.; Browne, W.; Mulligan, R.; Pike, K.; O'Keefe, G.; Tochon-Danguy, H.; Chan, G.; Berlangieri, S.; Jones, G.; Dickinson-Rowe, K.; Kung, H.; Zhang, W.; Kung, M.; Skovronsky, D.; Dyrks, T.; Holl, G.; Krause, S.; Friebe, M.; Lehman, L.; Lindemann, S.; Dinkelborg, L.; Masters, C.; Villemagne, V. Imaging of amyloid beta in Alzheimer's disease with (18)F-BAY94–9172, a novel PET tracer: proof of mechanism. *Lancet Neurol.* **2008**, *7*, 129–135.

(27) Zhang, W.; Oya, S.; Kung, M.; Hou, C.; Maier, D.; Kung, H. H. F-18 Polyethyleneglycol stilbenes as PET imaging agents targeting A $\beta$  aggregates in the brain. *Nucl. Med. Biol.* **2005**, *32*, 799–809.

(28) Zhang, W.; Oya, S.; Kung, M.; Hou, C.; Maier, D.; Kung, H. F-18 Stilbenes as PET Imaging Agents for Detecting beta-Amyloid Plaques in the Brain. *J. Med. Chem.* **2005**, *48*, 5980–5988.

(29) Koole, M.; Lewis, D.; Buckley, C.; Nelissen, N.; Vandenbulcke, M.; Brooks, D.; Vandenbergh, R.; Van Laere, K. Whole-body biodistribution and radiation dosimetry of 18F-GE067: a radioligand for in vivo brain amyloid imaging. *J. Nucl. Med.* **2009**, *50*, 818–822.

(30) Nelissen, N.; Van Laere, K.; Thurfjell, L.; Owenius, R.; Vandenbulcke, M.; Koole, M.; Bormans, G.; Brooks, D. J.; Vandenbergh, R. Phase 1 study of the Pittsburgh compound B derivative 18F-flutemetamol in healthy volunteers and patients with probable Alzheimer disease. *J. Nucl. Med.* **2009**, *50*, 1251–1259.

(31) Thomas, B. A.; Erlandsson, K.; Modat, M.; Thurfjell, L.; Vandenbergh, R.; Ourselin, S.; Hutton, B. F. The importance of appropriate partial volume correction for PET quantification in Alzheimer's disease. *Eur. J. Nucl. Med. Mol. Imaging* **2011**, *38*, 1104–1119.

(32) Vandenbergh, R.; Van Laere, K.; Ivanoiu, A.; Salmon, E.; Bastin, C.; Triau, E.; Hasselbalch, S.; Law, L.; Andersen, A.; Korner, A.; Minthon, L.; Garraux, G.; Nelissen, N.; Bormans, G.; Buckley, C.; Owenius, R.; Thurfjell, L.; Farrar, G.; Brooks, D. (18)F-flutemetamol amyloid imaging in Alzheimer disease and mild cognitive impairment: a phase 2 trial. *Ann. Neurol.* **2010**, *68*, 319–329.

(33) Vallabhajosula, S. Positron emission tomography radiopharmaceuticals for imaging brain Beta-amyloid. *Semin. Nucl. Med.* **2011**, *41*, 283–299.

(34) Jureus, A.; Swahn, B.; Sandell, J.; Jeppsson, F.; Johnson, A.; Johnstrom, P.; Neelissen, J.; Sunnemark, D.; Farde, L.; Svensson, S. Characterization of AZD4694, a novel fluorinated Abeta plaque neuroimaging PET radioligand. *J. Neurochem.* **2010**, *114*, 784–794.

(35) Pajk, S.; Pecar, S. Synthesis of novel amphiphilic spin probes with the paramagnetic doxyl group in the polar region. *Tetrahedron* **2009**, *65*, 659–665.

(36) Adamsen, T. C. H.; Grierson, J. R.; Krohn, K. A. A new synthesis of the labeling precursor for [18F]-fluoromisonidazole. *J. Labelled Compd. Radiopharm.* **2005**, *48*, 923–927.

(37) Qu, W.; Kung, M.; Hou, C.; Benedum, T.; Kung, H. Novel styrylpyridines as probes for SPECT imaging of amyloid plaques. *J. Med. Chem.* **2007**, *50*, 2157–2165.

(38) Rostovtsev, V. V.; Green, L. G.; Fokin, V. V.; Sharpless, K. B. A stepwise Huisgen cycloaddition process: copper(I)-catalyzed

regioselective "ligation" of azides and terminal alkynes. *Angew. Chem., Int. Ed. Engl.* **2002**, *41*, 2596–2599.

(39) Del Valle, J.; Duran-Vilaregut, J.; Manich, G.; Casadesu, G.; Smith, M. A.; Camins, A.; Pallas, M.; Pelegri, C.; Vilaplana, J. Early amyloid accumulation in the hippocampus of SAMP8 mice. *J. Alzheimer's Dis.* **2010**, *19*, 1303–1315.

(40) Beckmann, N.; Gerard, C.; Abramowski, D.; Cannel, C.; Staufenbiel, M. Noninvasive magnetic resonance imaging detection of cerebral amyloid angiopathy-related microvascular alterations using superparamagnetic iron oxide particles in APP transgenic mouse models of Alzheimer's disease: application to passive Abeta immunotherapy. *J. Neurosci.* **2011**, *31*, 1023–1031.

(41) Cheng, Z.; Wu, Y.; Xiong, Z.; Gambhir, S. S.; Chen, X. Near-infrared fluorescent RGD peptides for optical imaging of integrin alphavbeta3 expression in living mice. *Bioconjugate Chem.* **2005**, *16*, 1433–1441.

(42) Liu, Z.; Shi, J.; Jia, B.; Yu, Z.; Liu, Y.; Zhao, H.; Li, F.; Tian, J.; Chen, X.; Liu, S.; Wang, F. Two (90)Y-Labeled Multimeric RGD Peptides RGD4 and 3PRGD2 for Integrin Targeted Radionuclide Therapy. *Mol. Pharm.* **2011**, *8*, 591–599.

(43) Dijkgraaf, I.; Yim, C. B.; Franssen, G. M.; Schuit, R. C.; Luurtsema, G.; Liu, S.; Oyen, W. J.; Boerman, O. C. PET imaging of alphavbeta integrin expression in tumours with Ga-labelled mono-, di- and tetrameric RGD peptides. *Eur. J. Nucl. Med. Mol. Imaging* **2011**, *38*, 128–137.

(44) Dijkgraaf, I.; Kruijtzter, J. A.; Liu, S.; Soede, A. C.; Oyen, W. J.; Corstens, F. H.; Liskamp, R. M.; Boerman, O. C. Improved targeting of the alpha(v)beta (3) integrin by multimerisation of RGD peptides. *Eur. J. Nucl. Med. Mol. Imaging* **2007**, *34*, 267–273.

(45) Kiessling, F.; Huppert, J.; Zhang, C.; Jayapaul, J.; Zwick, S.; Woenne, E. C.; Mueller, M. M.; Zentgraf, H.; Eisenhut, M.; Addadi, Y.; Neeman, M.; Semmler, W. RGD-labeled USPIO inhibits adhesion and endocytotic activity of alpha v beta3-integrin-expressing glioma cells and only accumulates in the vascular tumor compartment. *Radiology* **2009**, *253*, 462–469.

(46) Li, F.; Liu, J.; Jas, G. S.; Zhang, J.; Qin, G.; Xing, J.; Cotes, C.; Zhao, H.; Wang, X.; Diaz, L. A.; Shi, Z. Z.; Lee, D. Y.; Li, K. C.; Li, Z. Synthesis and evaluation of a near-infrared fluorescent non-peptidic bivalent integrin alpha(v)beta(3) antagonist for cancer imaging. *Bioconjugate Chem.* **2010**, *21*, 270–278.

(47) Li, F.; Jas, G. S.; Qin, G.; Li, K.; Li, Z. Synthesis and evaluation of bivalent, peptidomimetic antagonists of the alphavbeta3 integrins. *Bioorg. Med. Chem. Lett.* **2010**, *20*, 6577–6580.